MODELLING MID-FREQUENCY SCATTERING AND REVERBERATION IN THE NORTHERN GULF OF MEXICO

A Thesis

by

Shannon-Morgan M. Steele

In Partial Fulfillment of the

Requirements for the Degree

of

Combined Honours Bachelor of Science in Earth Sciences and Oceanography

at

Dalhousie University

Halifax, Nova Scotia

April 2016

ACKNOWLEDGMENTS

I would like to thank my supervisor at DRDC, Dr. Sean Pecknold, for giving me a wonderful opportunity to work on this project. Over the past year Sean has taught me a great deal and has helped me discover my passion for underwater acoustics. Sean's patience, guidance, and support is truly appreciated. I would also like to thank my Dalhousie supervisor, Dr. David Barclay, for his advice and dedicated involvement throughout the process of writing this thesis. I am extremely thankful for his unwavering support.

TABLE OF CONTENTS

LIST OF FIGURES

Figure Page

SYMBOLS

TL	transmission loss
SL	source level
RL	recieved level
Sv	scattering strength
V	ensonified volume
σ_2	volume scattering parameter
$\sigma_r(\theta)$	roughness scattering cross section
$\sigma_v(\theta)$	volume scattering cross section
γ_1	1D spectral slope
ω_2	2D spectral strength
γ_2	2D spectral slope

ABBREVIATIONS

CRA	Composite Roughness Approximation
SAX99	Sediment Acoustics Experiment-1999
SAX04	Sediment Acoustics Experiment-2004
TREX13	Target and Reverberation Experiment-2013

ABSTRACT

Accurate sonar target detection requires the prediction of reverberation, which masks the target signal. Scattering and reverberation at mid-frequencies(1-10kHz) has not been as well studied as high-frequencies (above 10kHz). Thus, in this study, the validity of a high-frequency reverberation model for mid-frequencies was tested using environmental data collected during Target and Reverberation Experiment 2013 (TREX13). During the TREX13 sea trial it was observed that reverberation varied counterintuitively: with peak reverberation occurring within the troughs of the sand dunes. In order to investigate this spatial variation in reverberation environmental data collected during TREX13 was utilized in a high-frequency seafloor scattering model known as the composite roughness approximation (CRA). The results from this model were incorporated into a high-frequency reverberation model and compared to measured reverberation. Sub-bottom profiler data was used to visualize and quantify the spatial variation and physical mechanisms of scattering. Results from both the CRA and sub-bottom profiler indicate that volume scattering is the dominant scattering mechanism at mid-frequencies in the northern Gulf of Mexico. The peak scattering appears to be caused by the concentration of sub-surface volume scatterers in the transition zones between the peaks and troughs of the sand dunes. This study found the CRA empirical estimates of volume scattering underestimated the measured volume scattering, suggesting the CRA model should only be utilized for mid-frequency scattering if the volume scattering parameter can be calculated. This correction to the CRA model accurately predicts bottom reverberation, however the total reverberation model deviates significantly from the measured data, indicating that the other sub-models utilized in the reverberation model require validation for mid-frequencies.

1. INTRODUCTION

Sonar is one of the most important tools used for the exploration of the oceans. Sonar is particularly valuable for buried and proud object detection along the seafloor. In order to be able to accurately identify targets the mechanisms of sound behaviour in the ocean and the effect of environmental variability must be well understood. This proves to be a difficult task because the sound not only reflects off the target, it is also scattered by the seafloor, sea surface, and volumetric inhomogenieties (such as fish, suspended particles, and temperature gradients). This scattering causes an echo within the ocean known as reverberation. Reverberation masks the target signal and thus in order to improve target detection this reverberation must be quantified. Seafloor sediment scattering and reverberation at high frequencies has been well studied and quantified and there has been significant success in modelling backscatter from sediment at high frequencies. Mid-frequency scattering and reverberation, however, have not been as well studied. It is important that mid-frequency scattering and reverberation is understood because it allows us to detect objects below the seafloor: high frequency sonar can only propagate into the sediment at the centimetre scale, whereas mid-frequency sonar can propagate several meters below the seafloor. Currently, one of the greatest limitations on modelling reverberation at mid-frequencies is the prediction of seafloor scattering. In order to thoroughly investigate environmental effects on mid-frequency scattering and reverberation the TREX13 sea trial was conducted in the northern Gulf of Mexico. The purpose of this thesis is to test and adapt a popular high frequency scattering model and a reverberation model for mid-frequencies. In order to adapt the mid-frequency scattering model the mechanisms of mid-frequency seafloor scattering and reverberation must be understood. Thus this study will use environmental measurements of northern Gulf of Mexico seafloor bathymetry, sedimentology, and sub-surface geology to investigate the spatial variation in scattering and reverberation. This investigation of seafloor scattering will help improve our understanding of the physical mechanisms and environmental factors involved in seafloor scattering and reverberation.

1.1 Introduction to seafloor sound scattering and reverberation

If seafloor sediment was a perfectly flat, non-random, reflecting mirror, it would reflect all incoming energy at an angle equal to the angle of incidence [1]. However, seafloors are rough surfaces and often display some form of compositional heterogeneity, causing scattering. Scattering causes the sound signal to be reflected at angles other than the angle of incidence. Scattering from the seafloor is most commonly divided into two different types of scattering: sediment interface roughness scattering and sediment volume scattering. Roughness scattering is caused by seafloor roughness, which is primarily controlled by the shape and size of sediment grains as well as the topography (such as the presence of ripples or pock marks). Volume scattering is caused by sediment heterogeneity and discrete scattering from objects such as carbonate, shell hash, or fauna. The amount of energy scattered (seafloor scattering strength, S_b) depends on: the sediment geoacoustic properties, properties of the seawater at the sediment-water interface, acoustic frequency, angle of incidence, and angle of scattering [1]. As will be discussed in chapter 3, high frequency scattering in the northern Gulf of Mexico has been well studied. Since mid-frequencies penetrate far deeper into the seafloor than the high frequencies it is expected that the volume scattering will play a far more significant role in scattering than the minimal amounts observed for higher frequencies. Previous studies within the study area such as SAX99 and SAX04, will allow us to test this expectation. In the Geologic Background section (Chapter 3) the volume scattering mechanisms available in the northern Gulf of Mexico will be discussed.

The scattering resulting from the seafloor discussed above is of great concern for this study because it is a major contributor to reverberation. It is of particular interest for TREX13 because during the sea trial it was observed that the reverberation is higher over the troughs of the sand dunes, rather than the peaks, which is counterintuitive. Thus understanding the variation is seafloor scattering will allow us to understand the variation in reverberation. Reverberation is defined as the portion of sound received at a hydrophone that is scattered by ocean boundaries and volumetric inhomogenieties [2]. It is important to note that there is a key difference between ambient noise and reverberation: reverberation is produced by the sonar itself, causing reverberation spectral characteristics to be nearly the same as the transmitted signal. Ambient noise is not generated by the sonar system itself and will generally have spectral characteristics that are different from the transmitted signal. In addition to this reverberation intensity varies with the intensity of the transmitted signal, whereas the ambient noise will remain the same [2]. The intensity of reverberation varies with a large variety of factors including intensity of the transmitted signal, range from source to scatterers, sediment type, wind speed, and presence of fish just to name a few. According to Urick [3] this dependency on such environmentally dependent factors makes reverberation modelling formidable for two reasons: 1) There are theoretical difficulties in solving complex boundary problems, the tools for which are still being developed and 2) It is difficult to identify and measure all of the parameters affecting the reverberation process. Thus in order to be able to model reverberation there are five key assumptions that must be made:

1. Straight-line propagation paths with all sources of attenuation other than spherical spreading neglected. However, the effect of absorption on the reverberation level can be accommodated.

2. A homogeneous distribution of scatterers throughout the area or volume producing reverberation at any given time.

3. Sufficiently high density of scatterers to ensure that a large number of scatterers occurs in an elemental volume or area.

4. A pulse length short enough for propagation effects over the range extension of the elemental volume of area to be neglected.
5. Multiple scattering (reverberation produced by reverberation) absent.

To model scattering a successful high frequency model known as the Composite Roughness Approximation (CRA) was used. The CRA model was chosen because it divides sediment backscatter into interface roughness scattering and volume scattering, allowing us to isolate the volume scattering component and test the hypothesis that it is the dominant scattering mechanisms that causes both the spatial variation in reverberation and the difference between high frequency and mid-frequency scattering. In order to test the suitability of the current CRA model for use at mid-frequencies, data collected during the TREX13 sea trial will be used as inputs into a CRA model. The results from this model will be utilized in a reverberation model and compared to the measured reverberation. In order to investigate the mechanisms behind the surprising spatial variation in measured reverberation, sub-bottom profiler and cone penetrometer data will be used to analyze spatial variation in scattering. Based on the heterogeneous nature of the study area and deeper propagation depth of mid-frequency waves, it is expected that the volume scattering will be the dominant scattering mechanism, rather than the interface-roughness scattering dominance observed at high-frequencies [4], [5]. This indicates that the CRA model may not be able to properly model backscattering at mid-frequencies. Section 2 will describe our current understanding of how geoacoustic and geophysical parameters affect acoustic backscatter. Section 3 will provide an overview of the geological and acoustic properties previously measured in the northern Gulf of Mexico. In Section 4 bathymetry data collected during TREX13 and the calculation of the roughness interface parameter for the CRA model will be presented. In Section 4.3 geophysical properties measured by a cone penetrometer will be used to determine the geoacoustic parameters required for the CRA. The CRA model results will be analyzed and compared with both previously measured backscatter from sandy sediment in Section

4.4. Calculation of the volume scattering parameter, analysis of spatial variation and mechanisms of scattering based on the sub-bottom profiler data, and a comparison of the calculated scattering to scattering measured at high-frequencies during TREX13 will be presented in Section 5. Finally, in Section 6 the results of both the bottom reverberation and total reverberation models will be compared with the measured reverberation.

2. EFFECT OF PHYSICAL AND GEOACOUSTIC SEDIMENT PROPERTIES ON BACKSCATTER

The most important geoacoustic parameters utilized in backscattering modelling are sound speed ratio (which is the compressional wave speed) and attenuation. These types of measurements are difficult to obtain through direct measurement and therefore sediment physical properties such as mean grain size and porosity can be measured and used in empirical regressions to estimate values of geoacoustic parameters. Grain size is one of the most important physical measurement in backscatter modelling because it is relatively simple to measure and many sediment properties such as porosity, permeability, and wave speeds are very well correlated with grain size. In this study, in situ data collected by a cone penentrometer was used to determine sediment grain size, which, as will be discussed in Section 4.3, were used to determine many other inputs for the backscattering model. Sediments are often divided into two broad categories: fine grained sediment (mud, silt, and clay) and corse grained sediment (sands and gravel). Scattering from each sediment grain size can be highly variable but there are two general trends in backcattering and grain size that can be observed. The first is fine-grained sediments usually have lower roughness (and therefore lower backscatter), whereas coarser-grained sediments have highly variable roughness. The second trend has to do with the fact that fine grained sediment is known as slow because sound is refracted in the vertical direction, allowing it to penetrate deep into the sediment when compared to coarse grained(fast) sediment which refracts sound towards the horizontal [1]. In addition to horizontal variabilities in sediment properties it is important to note that there is a gradient in geoacoustic properties with depth. When sediment is buried the bulk density increases, porosity and permeability decreases, sound velocity increases, attenuation decreases.These compaction processes have been found to increase the scattering with depth [1].

3. STUDY LOCATION BACKGROUND

The TREX13 sea-trial was conducted in the northern Gulf of Mexico, just off the coast of Panama City, Florida, in an area often refferd to as Mississippi-Alabama-Florida (MAFLA) sand sheet. The location of the study has been indicated in the star in Figure 3.1. Data were collected in two different tracks known as the main track (shore parallel track) and the clutter track (shore perpendicular track). The rest of this section is a description of the geological and geoacoustic properties of the northern Gulf of Mexico.

Formation of the Gulf of Mexico

The Gulf of Mexico formed through seafloor spreading during the break up of Pangea. The seafloor spreading motion moving continental blocks and creating the Gulf of Mexico basin occurred from 160 to 140 Ma [6]. Prior to this breakup (approximately 180 Ma), numerous long, narrow-rift basins formed from the stretching of continental crust, creating topographically low valleys surrounded by uplands and mountains [7]. These rift-basins were eventually filled by a variety of sedimentary structures including alluvial fans, deltas, rivers, lakes, and shallow mud flats. Some of these basins are still present in modern topography, while others have been completely filled with sediments [7]. The Gulf of Mexico was significantly larger than it is today. The reduction in size was caused by a large mass of deposits during the Cenozoic [8]. The northern Gulf of Mexico shelf is referred to as a geosyncline composed of Cenozoic sediments [8]. The Gulf of Mexico has been described as a slowly subsiding, passive continental margin [9]. But it can also be described as an active passive margin due to salt tectonics [10].

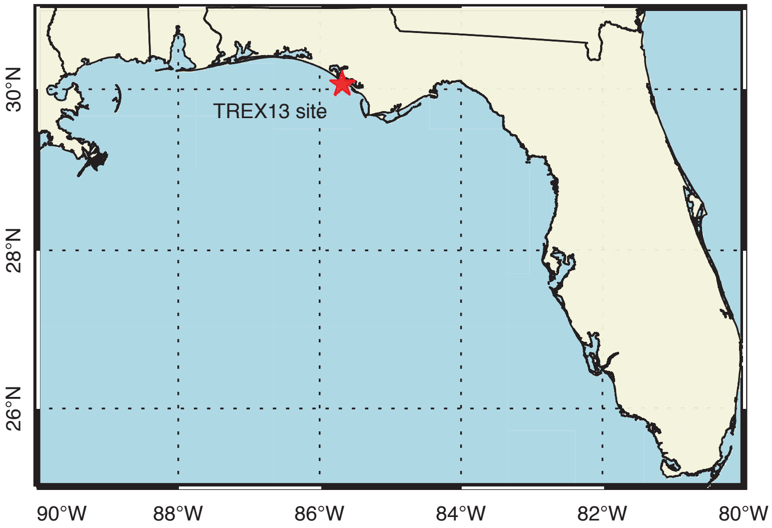

Fig. 3.1.: Map indicating TREX13 study location

Stratigraphy of the northern Gulf of Mexico

During the Triassic, following the formation of the Gulf of Mexico basin, a thick salt sheet was deposited on top of the syn-rift sediments of the young basin. During the late Jurassic the salt sheet was buried by continental sediment [10], [6]. Following this, the early Cretaceous facies was deposited. The early Cretaceous facies is composed of repeating sequences of carbonate separated by clay and sandstone [6]. On top of these sequences is a 2.5-3.5 km thick deposit of fine carbonate sediments from the late Cretaceous [6]. During the Neogene, tremendous volumes of terriginous sediment were deposited into the northern Gulf of Mexico, creating a thick (up to 16 km) continental margin [11]. The weight of the Neogene sediments caused the salt layer to begin to deform and move up and southward. This motion began during the Tertiary time and still continues today [10]. Most of the sediment found along the northern Gulf of Mexico shelf at the seafloor water interface is relict material, deposited during the last sea level low stand of the Pleistocene [12, 13]. The west Florida shelf has little active sedimentation today [14]. Therefore, most of the sediment analyzed in this study was deposited during the sea level oscillations of the Quaternary. During these oscillations several major episodes of deposition and erosion occurred along the shelf [9]. In particular, our study area is defined by marine sands up to 5.5 m thick that are underlain by a transgressive ravinement, followed by the Holocene muds and Pleistocene clay sand.

Core samples of our study area from Goff et al. [15] revealed that below the approximately 1.1 m thick top sediment of medium sand is a dense shell layer from approximately 1.1-1.6 m below the seafloor (a sample from a different area had the shell layer starting at approximately 0.4 m below the seafloor). Another layer of medium sand follows this shell layer. The upper sand contains relatively more shell hash, compared to the lower sand. The lower sand appears to contain fragments of woody debris and contains a much larger fraction of fine-grained sediment.

Sedimentology of the northern Gulf of Mexico

The seafloor sediments of the Gulf of Mexico continental shelf, offshore of Alabama-Florida, is mostly composed of sand, becoming progressively finer and muddier westward [9]. Since the Late Cenozoic most of these clastic sediments have been derived from fluvial transport originating in North America [16]. The gradient from sand to mud in the westward direction is attributed to the input of finer-grained, fluvial sediments from the Mississippi River and other river systems. Although our study site is not in close proximity to any major river systems, these rivers still contribute to the sediments through transport by deep marine currents [17], wind (surface currents) and tides [18].

In our study area, the sediment is dominated by unconsolidated, fine to medium-grained quartz sand that has a low carbonate content [13], [19]. The carbonate concentration in the sand sheet seems to vary amongst studies: [20] reported it as less than 25% Ludwick [21] describes it as less than 15%, and Fleischer [19] stated that it was 10% carbonate with some areas that are much higher due to the presence of shell fragments. Fleischer [19] reported the MAFLA sand sheet to have a thickness ranging from 2-10 m, however, the sediments begin to thicken starting 50 m out from the shelf [4]. Mineralogy and grain size change outward from the Alabama-Florida shelf. Clay mineral concentration increases away from the coast and the fine-grained quartz sand continue for about 80 km off the coast [20] before transitioning to calcareous sediment [12]. According to Doyle [20],our study area should be composed of 90% sand. It is important to keep in mind that examining sediments in the Gulf of Mexico at high resolution reveals that the detailed sediment distribution is patchy. Doyle [20] found that patches of very fine sediment (clay and mud) occurred frequently, and did not show a distribution pattern. They speculated that the reason behind this is related to the location's bathymetry. Similarly, Parker et al. [22] observed significant sediment type variation along the Alabama shelf on intervals less than 1km. It is also important to note that, due to major rivers and storms, sediment supply to the Gulf of Mexico fluctuates significantly [9]. Doyle [20] reported that the Gulf of Mexico sediments can undergo considerable textural and compositional changes, particularly during severe weather periods. According to a study by Kraft et.al [23], following Hurricane Ivan the shoreward region of the MAFLA sand sheet showed a net accumulation of approximately 1.6 m in sediment. The accretion of sediment exceeded 1m in 6-7 m waters and tapered off seaward to the 11-12 m isobath. Beyond this point evidence of seabed erosion can be found [24]. During the SAX04 study it was found that several storms (including Hurricane Ivan) significantly altered the sediment composition off the coast of Panama through the introduction of large quantities of mud. Over time it was found that most of this mud was transported away from the study site, however, some remained as interbedded deposits [25].

During the SAX04 experiment a mean grain size of 1.47 phi was calculated [25]. A study conducted by Mickey et al. [26] found the sediment in the northern Gulf of Mexico to be moderately to poorly sorted. Both Davis et al. [4] and Doyle et al. [20] reported that, in the northeastern Gulf of Mexico, poorly sorted sediment was more common closer to the continental shelf, slowly transitioning to moderately sorted further away. This observation is consistent with measurements taken during the SAX04 experiment, which found the sediment, just off the coast of Panama, to be moderately well sorted. Reed et al. [25] also found that the sand sediment off the coast of Panama showed homogeneous tortuosity. Gold et al. [17] reported the grains in this area to be angular. During the SAX04 experiment, it was found that both porosity and permeability of the sand samples had very little variability [25]. Tang et al. [5] calculated the average porosity in the top 25 cm to be 0.372 with a coefficient of variation below 1%: indicating that the sediment is very homogeneous, with most of the variation in the surface layer (top 6mm). During the SAX99 experiment Buckingham et al. [27] reported the fractional porosity of the sediment to be 0.38, indicating that the grains in medium and coarse sand can be modelled as a random packing of smooth spheres. Tang et.al [5] also found that the wet bulk density of sediment off the coast of Mexico experienced small variations with an average of 2.065 g/cm .

Mineralogy of the northern Gulf of Mexico

Although the top sediment in our study area is composed mostly of quartz sand, there is a large suite of minerals that can also be found in cores taken of the northeastern Gulf of Mexico. Ludwick [21] has described the sediments of the Mississippi River Delta east to Cape San Bias as a series of clastic sand, mud, and transitional facies. The northeastern Gulf of Mexico can be characterized by a relatively high amount of ilmenite, staurolite, kyanite, zircon, and tourmaline [4, 17]. Samples from the northeastern Gulf of Mexico also contained minor amounts of leucoxene, epidote, amphiboles, biotite, sillimanite, dolomite, and pyroxenes [20], [17]. Gold et al. [17] described this as a metamorphic mineral assemblage that was likely derived from the Appalachians, either directly from the bedrock or from surfficial deposits of the Pleistocene. Mud can also be found in the sediment of the northeastern Gulf of Mexico. Both kaolinite and smectite can be found in the study area. Doyle and

Sparks [20] also found that there was anywhere from trace amounts to 16% illite. Relative concentrations of clay minerals vary depending on location. In general, the ratio of kaolinite to smectite increases eastward from the Mississippi River to the Apalachicola river, with intermediate compositions in between [20], [18]. Doyle and Sparks [20] also found that smectite concentration decreased and kaolinite increased dramatically towards the shore. Based on both these spatial variations, it is expected that clay in our study area should be have an intermediate composition of smectite and kaolinite, with a higher concentration of kaolinite. It should be noted that Doyle and Sparks [20] also found that ratios of kaolinite and smectite show distinct and frequent temporal variation. This temporal variation was seen between the SAX99 and SAX04 experiments. During the SAX99 experiment the sediment was described as nearly homogeneous sand sediment [28]. However, due to hurricane and other storm activity SAX04 observed a significant amount of mud in the sediments that, as discussed earlier, were eventually swept away from the site [28]. The organic content in our study area is low (0.3 to 0.77%) and is usually found in the shallow troughs of the sand ripples [28]. The presence of methane bubbles in the MAFLA sand sheet has not been reported.

Structural, Topographic and Bathymetric Properties of the Gulf of Mexico

The Mississippi-Alabama shelf is broad and nearly flat, the shelf edge is identified by a gradual increase in slope over several kilometers. The width of the shelf ranges from 122 km to 44 km, with an average of 95 km [22]. The structure of the Gulf of Mexico is complex and is characterized by deformational processes that can be distinguished in both the surface and subsurface. These include faulting, erosion, folding, mass movement features, and bioherms [16]. These deformations have been caused by steep slopes, diaperism, and faulting from instabilities and mass movements [16]. Surface features identified in the northern Gulf of Mexico include shoals, sand sheets, scarps, and sand waves [9]. A study completed by Fleischer [19] found north trending sand waves(large-scale ripples) that were generally symmetrical, with amplitudes between 1 and 3 m. The spacing between the sand waves ranged anywhere from 100-200 m. The sorting along these sand waves was considered well sorted. Parker [22], conducted a study of topography approximately 25 km south of Morgan Peninsula (west of our study site) and obtained similar results. They found series of north and northwest trending sand waves with highly variable geometry: crests could be symmetric or asymmetric, amplitudes ranged between 1 to 4 m, average spacing between waves was 0.5 km, length was anywhere between 0.31-2.65 km, and crest lines ranged from straight to curved. The variability of seafloor topography was found to be coincident with variations in sediment textures (grains were well sorted). Large-scale ripples have also been reported in the more recent SAX04 experiment. Goff et al. [15] reported NW-SE trending ripples with amplitudes of 1-2 m, but only found them in the NW sector of our study area. Goff et al. [15] reported that the sand ridges lie on approximately 45 °angle with the shoreline.

On a much finer scale, topographic features (such as ripples) that are of the size of mid to high frequency waves are non-existent or in some cases so smooth and decaying that they are not well detected. The lack of small scale topography produces a roughness spectra with a very steep slope [28]. During the SAX99 experiment it was found that the roughness spectrum had considerable variation.The deviations from the regression indicate that the spectrum slope and strength should be determined from spatial frequencies pertinent to the acoustic wavelength of interest. Where small scale ripples are present (amplitudes of 2:3 cm)show areas of uniform reflectance regions (possibly representing smaller sized sand grains) along the crests, and speckled regions (possibly representing larger grains and shell particles) inside the troughs. Parker [22] reported finding small bed forms caused by storms. Following storms,the settling of suspended mud often results in the formation of sand lenses [29]. Similarly, Pyle [30] reported a variety of topography ranging from giant sand waves, large sand waves, low relief swells and irregular hummocky bed forms.

Geoacoustic Properties of the northern Gulf of Mexico

A side scan sonar study performed in the northeastern Gulf of Mexico by Davis et al. [4] found that there was a high, direct correlation with the mean grain size of the sediments and acoustic backscatter. They also found that the carbonate content of the sediments influenced backscatter. It is likely that carbonate affects both mean grain size and roughness spectra because their flat surfaces and many angles make them more effective at backscattering acoustic energy than other sediment grains. Davis [4] found that, although volume scattering appeared to contribute to the backscatter, at high frequencies (above 10 kHz), backscatter is controlled primarily by roughness spectra. Previous to this Stanic [31] found a similar result, stating that at high frequencies, scattering occurs primarily at the sediment-water interface and does not penetrate far into the sediments. Tang et al. [5] found that in the northern Gulf of Mexico, any volume scattering present was mostly generated by spatial variability in sediment density or sound velocity. During the SAX99 experiment Tang et al. [5] reported that the horizontal 1D spectra generally follow a power-law form (ranging from 1.72 to 2.41) up to depths of 4 cm. Beyond this depth the spectral exponent decreases. The vertical 1D spectra also followed the power law but it had an exponent of 2.2. Tang et al. [5], found the greatest variability of sediment conductivity, porosity, and density in the top 4-5 mm. Tang et al. [5] reported that the sound speed ratio and density coefficients of variation indicate that the sediment in the northeastern Gulf of Mexico is relatively uniform. These results indicate that sediment volume variability below the interface transition should not significantly impact acoustic backscatter at frequencies below 100-150 kHz. Above 100 kHz sediment volume variability within the interface transition plays an important role in scattering [5].

In terms of spatial variation it has been shown that over large areas backscattering in the northeastern Gulf of Mexico display regions of both gradual and abrupt changes in seafloor backscatter strength [4]. However, on a large scale, it has been found that acoustic scattering is nearly isotropic [4]. These spatial variations in backscatter are generally attributed to variations in sediment composition. Davis [4] found that the mean relative backscattering strengths of the fine, medium, and coarse sands were approximately 9.8, 17.2, and 24.7 dB , respectively. Davis [4] also reported that the variability of backscatter strength from fine grained sands is twice that associated with medium and coarse grained sands. This may be attributed to the random occurrence of shell material in the fine sand [32]. In their experiment, Parker et al. [22] found that predominantly quartz sand facies (such as those expected to be observed in our experiment) created moderate to weak backscatter. This backscatter was increased to strong by the presence of carbonate (shells). Sediment containing mud, carbonate and sand showed moderate to strong backscatter.

In addition to spatial changes in backscatter there is also temporal variations of backscatter in the northern Gulf of Mexico. Richardson [28] found that the MAFLA sand sheet long-term temporal and large-scale spatial variability in acoustic scattering is controlled by hydrodynamic processes, while biological processes control short-term temporal and small-scale spatial variability. However, short term temporal variations may be controlled primarily by weather events. During the SAX04 experiment it was found that after the passing of Hurricane Ivan there was a threefold increase in root mean square (rms) roughness parallel to the shore at shallow depths. Perpendicular to the coastline it was noted that rms roughness increased between 3 and 4 times at depths of up to 20 m. This increase in scattering was attributed to volume scattering caused by the presence of mud lenses discussed previously.

Other than scattering there are many other geoacoustic studies that have been conducted in the northern Gulf of Mexico, which are important for modelling seafloor scattering. Values of compressional and shear wave velocity are much lower in muddy compared to sandy sediments, however no significant difference between coarse and fine sand was found [33]. In their experiments, Fracncisca et al. [34] found that all their study sites in the northern Gulf of Mexico had approximately constant shear wave velocities with depth (except near carbonates). Similarly, during the SAX99 experiment, Tang et al. [5] and Buckingham and Richardson [27] found that sediment sound-speed experienced only small variations with depth, increasing weakly with depth beneath the seawater-sediment interface. During the SAX99 experiments Buckingham and Richardson [27] calculated that, at 38 kHz, the mean compressional wave sound speed is 1778 m/s and the mean attenuation is 12 dB/m. However, it is important to note that compressional wave velocities are much higher in surficial sediments than in the water and attenuation values are very high [33]. Buckingham and Richardson [27] also determined dispersion of broadband measurements between 25 and 100 kHz to be weak but detectable and the attenuation scales almost linearly with frequency. In the presence of methane bubbles shear wave propagation is nearly unaffected but compressional waves scatter significantly and become difficult to detect [33].

Overall there seems to be two distinct types of sediment on the MAFLA sand sheet that we should expect to observe in the TREX13 study area: a highly reflective, coarse-grained, sand containing shell fragments, coralline algae and mollusk shells, and a weakly reflective, fine-grained sand with occasional muddy layers or inclusions [33], [32].

4. BACKSCATTERING MODEL

4.0.1 Model theory

To model backscatter in the northern Gulf of Mexico the Composite Roughness Approximation(CRA) [35]. was used. The CRA has two different components: the interface roughness cross section($\sigma_r(\theta)$) and the sediment volume scattering cross section($\sigma_v(\theta)$). Both of these cross sections are dimensionless and are described as backscattering cross section per unit solid angle per unit area [35]. The main basis of the CRA is that it is divided into the small scale and large scale components of scattering. The small scale portion of scattering is from the seabed roughness. Small scale roughness features are those that are on scales smaller than that of the acoustic wavelength. The large scale portion of scattering alters the grazing angle and causes acoustic shadowing, which must be corrected for. Large scale roughness features are those that are the same size as or larger than the acoustic wavelength (such as the ripples observed in our study area). The wave number that defines the boundary between large and small scale roughness is the cutoff wavenumber. In addition to the small and large scale parts the roughness scattering also requires the Kirchoff approximation to be calculated. The small scale component is calculated using the small scale roughness perturbation approximation, which is an approximation to the slope averaging integral. The large scale roughness is calculated using the large-roughness scattering cross section and the shadowing correction.The volume scattering is calculated using the shadowing correction as well as the small roughness perturbation approximation. The organization and flow of the CRA model approximations can be observed in Figure 4.1. The CRA model makes two important assumptions: 1) The statistics are spatially stationary, meaning that the roughness statistics are large

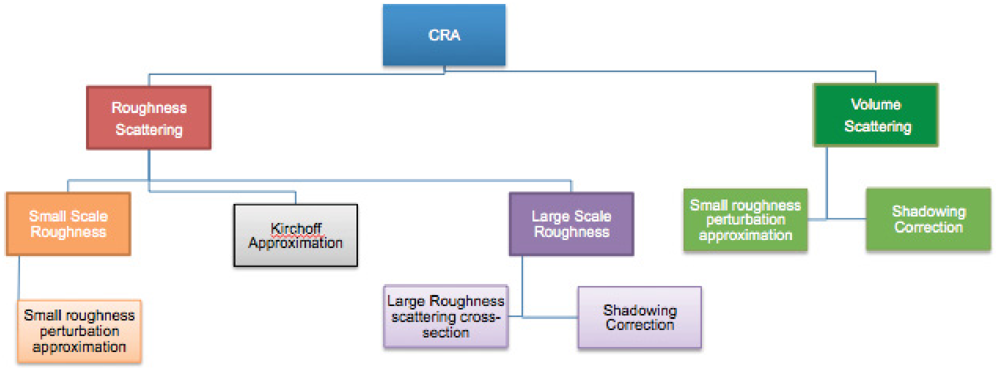

Fig. 4.1.: Flow chart demonstrating the organization and flow of the CRA model

compared to the area ensonified by the sonar and thus the statistics are independent of the location they were collected. 2) The data abides Gaussian statistics [35].

This CRA model is based off of the first-order perturbation theory for the Biot wave theory, as described in [1]. The Biot model describes the wave theory for the poroelastic case. The Biot theory treats the sediment as a two-phase system composed of grains and water. Dividing the sediment into two different phases: fluid(water) and shear supporting frame(grains) is important because each of these components may behave differently in the presence of waves. This coupling causes the acoustic wave of the fluid and the compressional and shear waves of the frame to combine into three hybrid wave types: two with longitudinal displacement and one being a shear wave with transverse displacement and two different polarizations [1].The fluid and frame move in the same direction for the fast (p) wave but in opposition for the slow(s) wave [1]. A more detailed analysis of the CRA model physical theories can be found in [1].

In order to compute backscatter the model requires the following input parameters: loss parameter, density ratio, velocity ratio, two-dimensional spectral strength and slope, volume scattering parameter, and cutoff wavenumber. The density ratio and velocity ratio are represented by the ratio of water to sediment density and velocity. The loss parameter, density ratio, velocity ratio, and volume ratio can be determined from the cone penetrometer results discussed in Section 4.3. According to the APL-UW the volume scattering parameter can be empirically estimated based on grain size. The spectral strength and slope are used to calculate the interface roughness scattering, and are derived from the area bathymetry. The methods for the calculation of these parameters are described in the next section.

4.1 Bathymetry data and calculation of spectral strength and slope

The TREX13 bathymetry data utilized in this study was collected in two different areas known as the main track (Figure 4.2) and clutter track (Figure 4.3).There are three different types of bathymetry sources that provided a total of seven sources of bathymetry data to be analyzed. Three of which were collected at 10 m resolution, one at 7.5 m resolution, two at 1m resolution and one at resolution less than 1m. In order to better visualize the geometry of the bathymetry side profiles of the bathymetry in both the along track and across track directions have been plotted.

4.2 Results

As expected, when looking at the shore parallel profile of the main track(Figure 4.4(a)), one can see large scale(0.5-1.5 m amplitude and 250-500 m wavelength), north-south trending sand ripples. The sand ripples appear to be most prominent westward with their frequency increasing and wavelength decreasing toward the east until they eventually flatten out. The clutter track shore parallel bathymetry side profile(Figure 4.5(a)) is relatively smooth but appears to have waves of the same scale as the shore parallel main track bathymetry. In the shore perpendicular direction (Figure 4.5(a))the main track is flat with a gentle slope towards the centre of the basin. Along the clutter track the bathymetry of the shore perpendicular direction(Figure 4.5(b)) has sand waves of similar scale to those described parallel to the shore in the

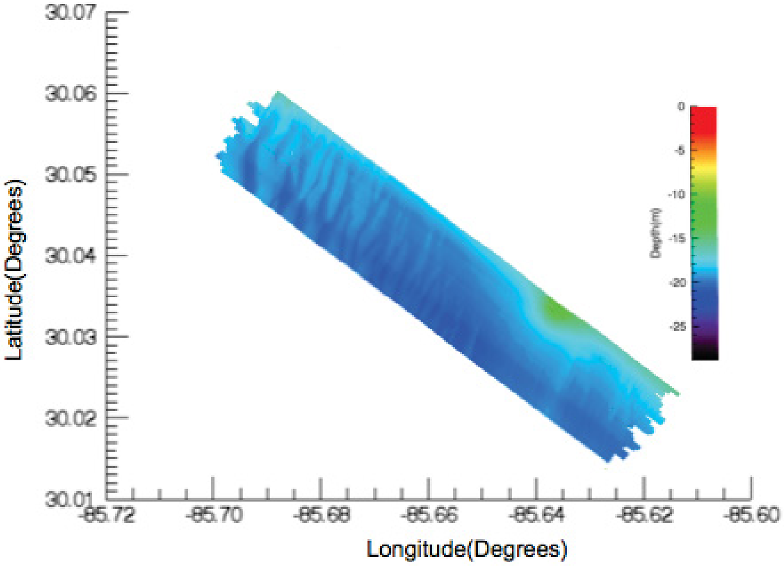

Fig. 4.2.: Bathymetry of Main track

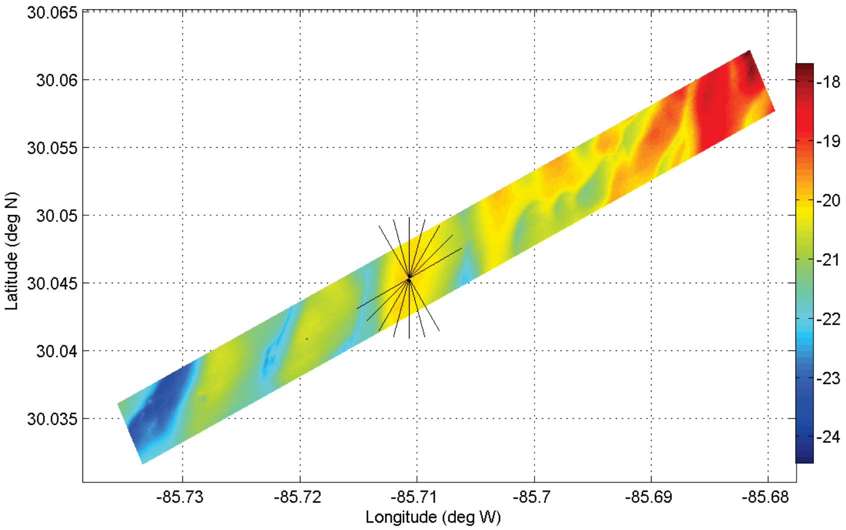

Fig. 4.3.: Bathymetry of Clutter track

clutter tack, however the variation in size is much larger and the ripples are sloping down towards the basin.

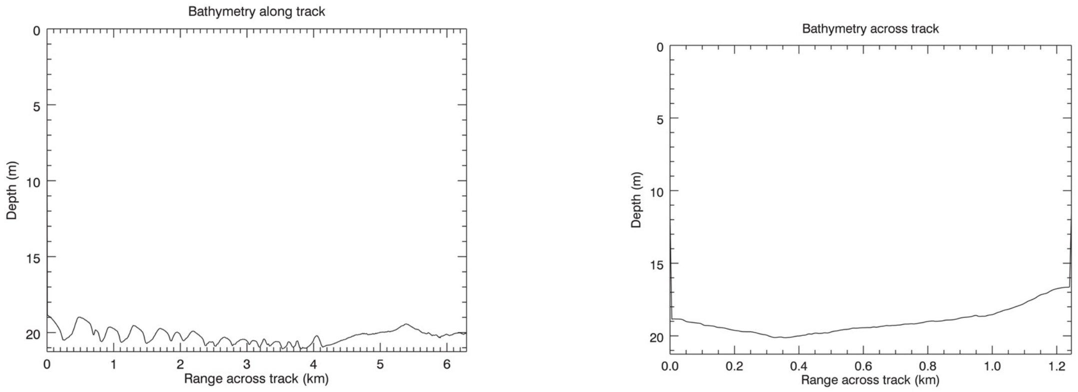

(a) Shore parallel direction at 1m resolution

(b) Shore perpendicular direction at 1m resolution.

Fig. 4.4.: Bathymetry profiles of main track in two different directions.

4.2.1 One-dimensional spectra

The bathymetry analyzed above was used to calculate the one dimensional roughness spectra in both the shore parallel and shore perpendicular directions of the main track and the clutter track. The various sets of bathymetry data were interpolated onto an evenly spaced grid in order to calculate the roughness spectra. Due to quality control issues one set of bathymetry data was not used (the bathymetry had values ranging from -600 to 20 m, which is not a possible range of values in our study area). The following process was followed for each bathymetry set: for each line in a direction a periodogram was calculated and then all the periodograms for a direction were averaged. Finally all of the periodograms were averaged to produce one average periodogram. Before computing the periodogram the data was pre whitened, the slope was removed, and a Hanning window was preformed. Following the Fast Fourier

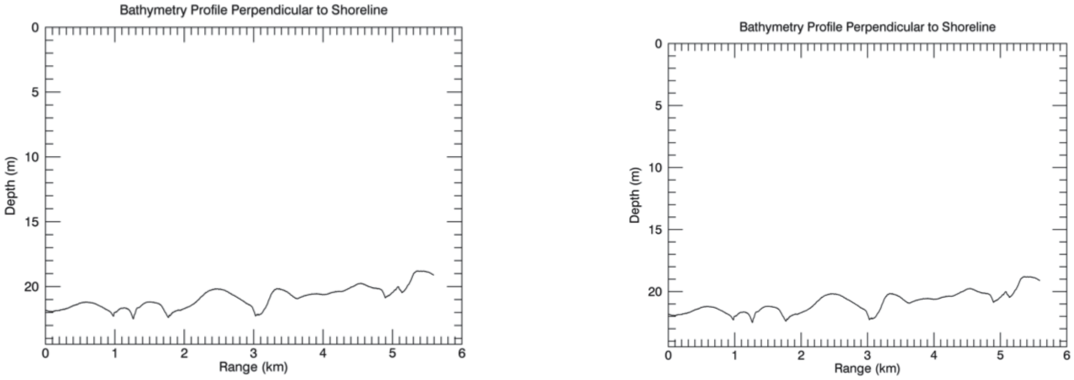

(a) Shore parallel direction at 1m resolution

(b) Shore perpendicular direction at 1m resolution.

Fig. 4.5.: Bathymetry profiles of clutter track in two different directions.

Transform (FFT) the pre whitening was corrected for. The resulting spectra have all been plotted in Figure 4.6. Some of the spectra have much higher than expected noise level. This is caused by either areas in the data where values are missing so the bathymetry value was assigned zero or in some datasets the zero values surrounding the image caused the interpolation to be distorted. Figure 4.6 shows that the spectra of the study area is highly variable, however, they all have very similar slopes. The high variation and steep slopes observed in Figure 4.6 are a result of a lack of fine scale topography (i.e. a relatively smooth surface at the scale of interest).

4.2.2 Two-dimensional spectra

The computation of the spectral strength and spectral slope assumes the sediment is isotropic. Thus, in order to test that this is a reasonable assumption a two-dimensional FFT was calculated for each dataset. Since isotropy is scale dependent, the 2D spectra were calculated at multiple different scales. When calculated over very large areas (0.5 to 1 km scale) the 2D spectra show that that there is in fact

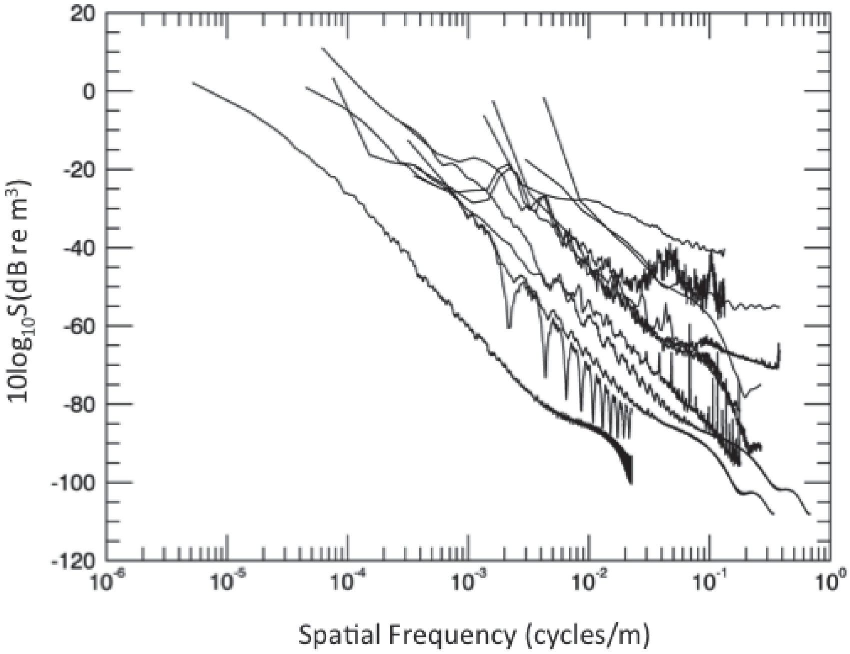

Fig. 4.6.: One-dimensional roughness spectra calculated from both directions from both the main track and the clutter track

some directional dependency, which likely correspond to the large scale ripples seen in the bathymetry. An example of 2D spectra showing directional dependency over the distance of 550m can be seen in Figure 4.7(a) However, at the fine scales that are of interest when studying mid to high frequency acoustic backscatter, the sediment is roughly isotropic (Figure 4.7(b)). In this study it has been assumed that the sediment is isotropic enough to treat it as isotropic, but in future studies this assumption should be further tested. It is important to note that the square (instead of circular) nature of the 2D spectra shown in the figures below is likely due to windowing.

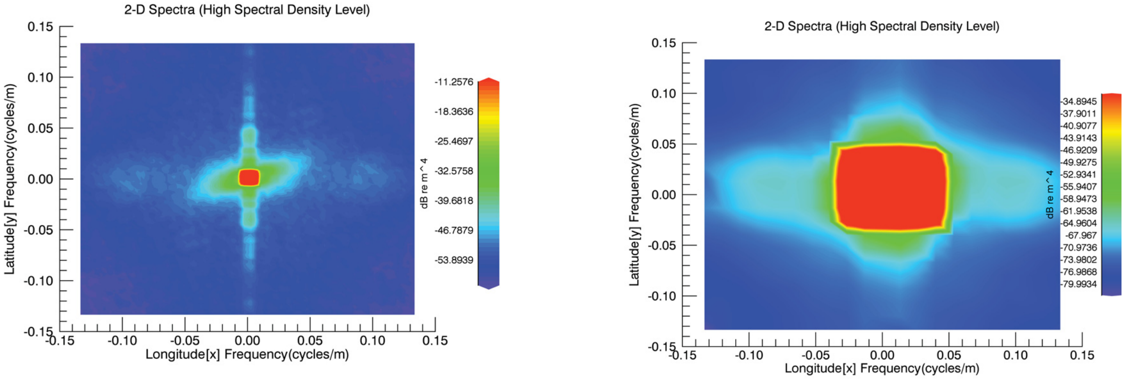

(a) Directional dependent spectra when sampled at 550m

(b) Isotropic spectra when sampled at 75m

Fig. 4.7.: Two dimensional spectra from the main reverberation track indicating how sediment isotropy increases with decreasing sample areas.

4.2.3 Spectral strength and spectral slope

Using the methods described in [35], the roughness spectra calculated in 4.2.1 were used to calculate the spectral strength(ω_2) and spectral slope($-\gamma_2$). To calculate these parameters the spectra plotted in 4.6 were averaged and the power law fit to the average curve was calculated. Since, in this study, we found the roughness to be isotropic the spectral strength and slope can be determined from the 1D spectra, which is modelled as a power law of spectral strength (ω_1) and slope($-\gamma_1$). Using

$$\gamma_2 = \gamma_1 + 1 \tag{4.1}$$

and

$$\omega_2 = \frac{\omega_1 * \Gamma\left(\frac{\gamma_2}{2}\right)}{\sqrt{\pi}\frac{\Gamma(\gamma_2-2)}{2}} \tag{4.2}$$

The spectra can be expressed in the 2D power law form:

$$W(\vec{k}) = \omega_2 k^{-\gamma_2} \tag{4.3}$$

The power law fit for the shore perpendicular lines was $\omega_1 = 5.772^{-7} m^{4-\gamma_1}$ and $\gamma_1 = 0.997$. yielding 2D spectral strengths and slopes of $\omega_2 = 5.386^{-9} m^{4-\gamma_2}, \gamma_2 = 1.997$. The power law fit for the shore parallel lines was $\omega_1 = 1.752^{-6} m^{4-\gamma_1}$ and $\gamma_1 = 1.609$, with 2D spectral strength and slope of $\omega_2 = 3.009^{-7} m^{4-\gamma_2}$ and $\gamma_2 = 2.609$. The power law fit obtained from the average of all the 1D spectra is $\omega_1 = 5.716^{-8} m^{3-\gamma_1}$ and $\gamma_1 = 1.454$. The average 2D spectral parameters were calculated to be $\omega_2 = 4.464^{-7} m^{4-\gamma_2}$ and $\gamma_2 = 2.454$. The average 1D spectra and the power law fit for the spectra can be seen in Figure 4.8.

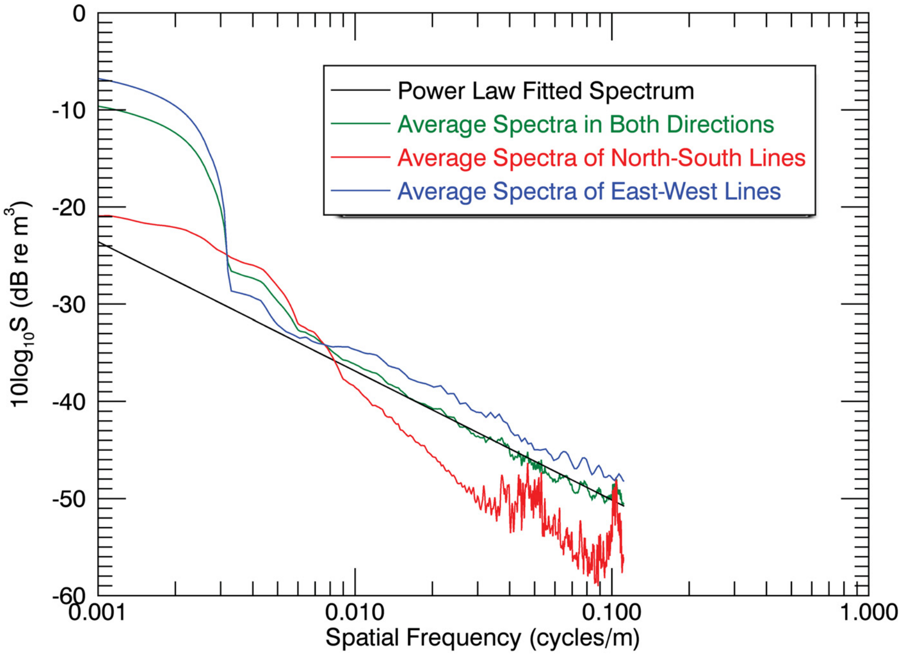

Fig. 4.8.: Average one-dimensional spectra in the north-south direction, the east-west direction, over all directions, and the power law fit to all the one-dimensional spectra.

4.3 Cone penetrometer analysis

The cone penetrometer data was collected over two different days on both the clutter track and the main track. The cone penetrometer data was analyzed using FFCPT View by Brooke Ocean Technology. The data was analyzed multiple times using different input parameters. This was done in order to help generate drops with the least amount of sediment that cannot be classified in the Robertson plot. The Robertson plot defines different acoustic sediment types as a function of FFCPT cone resistance and friction ratio (pore pressure parameter). The plots were first calculated using the default input parameters of FFCPT View and then changed based on the findings of past literature. The input parameters are: cone factor, pore pressure factor, undrained shear strength ratio, and saturated unit weight. The final parameters that were used are as follows: undrained shear strength=0.27, cone factor=14.0, saturated unit weight=17.0, pore pressure=14.0. Provided below is a description of all these parameters and the reasoning for choosing each parameter value.

Cone factor

Cone factor is correlated to the plasticity index of the sediment. A cone factor of 14.0 was used because according to a study done on sediments in the Gulf of Mexico the Cone Factor was measured to be between 10-15 [36] and according to Kim [37] the preliminary estimates of cone factor should be between 14 and 16.

Undrained shear strength

Shear strength is the magnitude of shear stress that a sediment can sustain. Undrained shear strength depends on the initial void ratio (initial water content) of the sediment. It is mainly controlled by sediment type and consolidation. For shear strength a value of 0.27 was used because sands and silty sands have a typical undrained shear strength range of 0.25-0.29.

Pore pressure factor

Pore pressure is the magnitude of pressure exerted by the fluids within the pores of the sediment as well as the pressure exerted by the overlying water. According to Mosher et al. [38] a pore pressure factor of 12-18 should be used in clays and a study conducted in the Gulf of Mexico found the average pore pressure value to be 12 [36]. Through testing in this dataset a value of 14 seemed to be most suitable.

Saturated unit weight

Saturated unit weight is defined as the unit weight of a sediment when all void spaces of the soil are completely filled with water. According to Mosher et al. [38] a value of 17 kN/m^3 is a suitable value for saturated unit weight of loosely consolidated sands and muds. In this study a value of 19 kN/m^3 seemed to be the most suitable.

4.3.1 Cone penetrometer results

All of the drops collected in the clutter track did not penetrate the sediment enough to detect sediment composition. This indicates that gravel, hard-packed sand, shell hash or other discrete scatterers were present in this area. This frequency of non penetration events indicate that discrete and volume scatterers are very dense in the clutter track and thus volume scattering may play an even more significant role in sediment backscatter on the MAFLA sand sheet than what was originally expected. This is particularly true at mid-frequencies, but such considerations should also be taken with high frequency scattering as well because the cone penetrometer rarely penetrated deeper than 30 cm into the sediment of the clutter track before falling over. The main track cone penetrometer profiles reflect a sediment composition that is consistent with previous observations of MAFLA sand sheet composition: fine to medium grain sands with patches of fine grained sediment(mud and silt). However, it is important to note that this area also had a significant amount (50%)of drops that resulted in non-penetration events. In previous studies fine sediment distribution was often described as random or sporadic, however, as observed in figure 4.9, the cone penetrometer data indicates a pattern of fine grained sediment (fine to medium sand and silt) in the troughs of sand waves and coarse grained sediments (medium to coarse sands and gravel) on the peaks. The average mean grain size determined from the cone penetrometer data was -0.8 which corresponds to very coarse sand. This result of very coarse sand rather than medium sand is likely to do with the presence of large scatters such as gravel, as well as the fact that the cone penetrometer does not differentiate between different types of sand because it uses a Robertson plot. From the mean grain size the following parameters were calculated according to methods from the APL-UW 94' handbook [35]: Sound speed ratio between water and sediment at the sediment-water interface(υ)=1.23; Density ratio between water and sediment at the sediment-water interface (ρ)=1.46; volume scattering parameter (σ_2)=0.02; cutoff wavenumber (k_c)=0.1cycles/m ; and loss parameter (δ)=0.016. These were then inputed into the model outlined by the APL-UW '94 handbook [35].

4.4 CRA model results

In Figure 4.10 the CRA model of backscattering strength has been plotted along with Lambert's law and the Lambert's law fit for sandy sediment(μ=-20.2), as calculated by [1]. The model predicts a roughness scattering peak at near vertical incidence and again near the critical grazing angle (35.7 degrees). Backscattering decreases as grazing angle becomes smaller than the critical angle. At all grazing angles, except normal incidence (90 degrees), the model is dominated by volume scattering. The roughness backscatter has the greatest influence at around normal incidence and at very low grazing angles (near zero). Between 90 degrees and the critical angle the

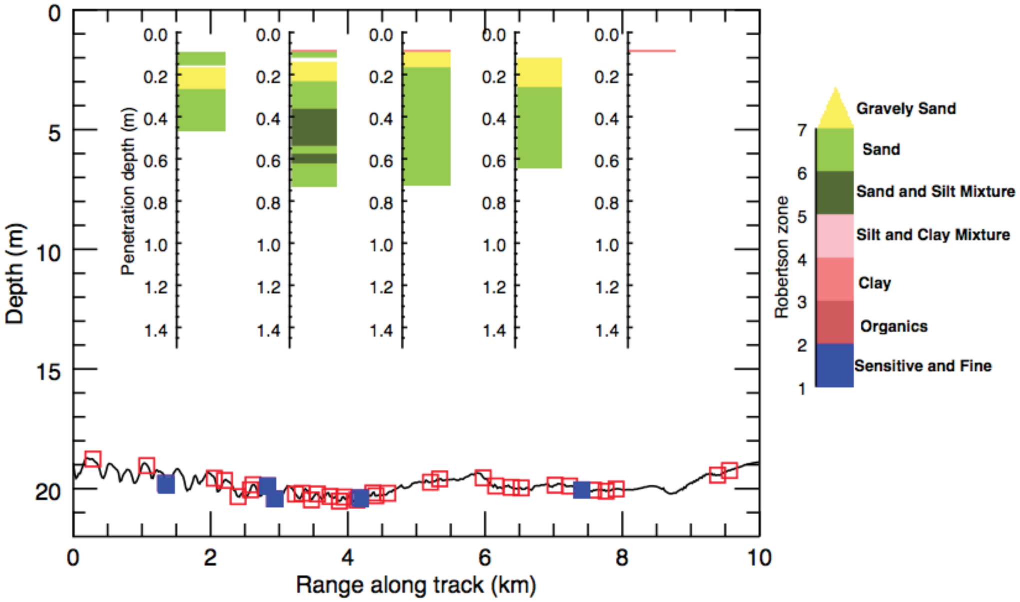

Fig. 4.9.: All the successful cone penetrometer drop locations (squares) plotted along the shore parallel direction of the maintrack bathymetry. Profiles of selected cone penetrometer drops (blue squares) are used to illustrate that the coarser grained sediment is found on the peaks of sand waves and finer in the troughs. Note that each profile left to right corresponds to each blue square plotted left to right.

model shows a similar shape to that predicted by Lambert's law. An important characteristic of this shape is the low dependence of scattering levels at angles approaching the normal incidence [3]. At the critical angle the scattering increases slightly and then demonstrates a steep slope, causing the backscattering strength to be much lower than what is predicted by Lambert's law. This relatively steep slope continues until about 15 degrees where the CRA plot has a much smaller slope than predicted by Lambert's law. With an intercept at -9 dB, the CRA model predicts scattering that is almost two full orders of magnitude greater than Lambert's law, and nearly a full order of magnitude higher than the Lambert's law for sandy sediment. However, it is important to note that the original spread of the data in the Lambert's law fit to sandy sediment was ±5 dB [1], thus indicating that the intercept for the Lambert's law fit for sandy sediment and the CRA model are somewhat similar. This difference between the two may be due to the fact that the Lambert's law fit for scattering to sandy sediment was for data collected at high-frequencies. One of the greatest downfalls for the CRA model is the use of an empirical estimate of volume scattering based on grain size, which is not necessarily an appropriate indicator of volume scattering. In order to test the validity of this empirical method the volume scattering coefficient will be calculated from the sub-bottom profiler and the spatial variation of scattering will be examined.

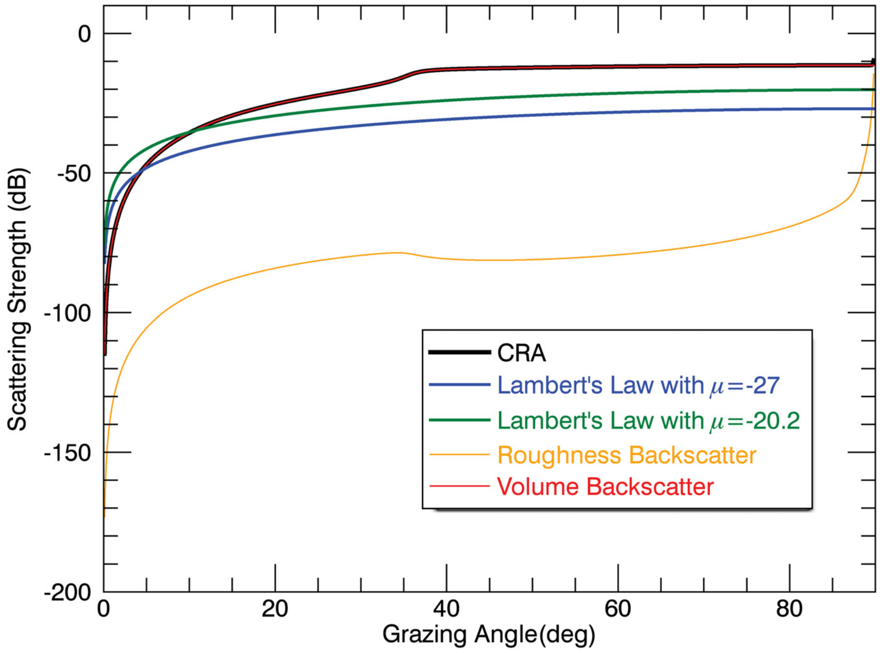

Fig. 4.10.: Plot comparing scattering strength as function of grazing angle for: the CRA model of TREX study area, Lambert's Law($\mu = -27$) and Lambert's Law fit for sandy sediment($\mu = -20.2$). Also shown is the roughness interface scattering strength and the volume scattering strength components computed for the CRA.

5. SUB-BOTTOM PROFILER ANALYSIS AND VOLUME SCATTERING

5.1 Qualitative volume scattering analysis

The X-Star sub bottom profiler data was computed and visually analyzed at regular intervals. A plot of the match-filtered return signal from the entire main track can be seen in Figure 5.1. In Figure 5.1 it appears that the troughs of the sand waves have very low attenuation (i.e. more of the sound energy propagates deeper into the sediment before being reflected). This phenomenon can be explained by the cone penetrometer data, which, as discussed earlier, indicated that the troughs were mostly composed of finer grained sediment (silts and sandy silts). As discussed in Section 2, finer grained sediments typically have much higher attenuation and lower reflection. Circled in Figure 5.1 are examples of discrete volume scatterers. The discrete scatterers appear to be most highly concentrated in the last 2 km of the track which corresponds to the flat area of the bathymetry. However, it is important to note that the scatterers can be found frequently throughout the seabed. Most are located around 1.5 to 2 m below the sediment water interface. In addition to the horizontal variation observed from the cone penetrometer data there is also significant sediment inhomogenieties with depth, with several layers of sediment appearing within the first few meters. These layers have been indicated by the arrows on the sub-bottom profiler image in Figure 5.1. In the next section this sub-bottom profiler data will be used to calculate the contribution of volume scattering at mid-frequencies. The parameter derived from this data will be used as an input for the CRA model.

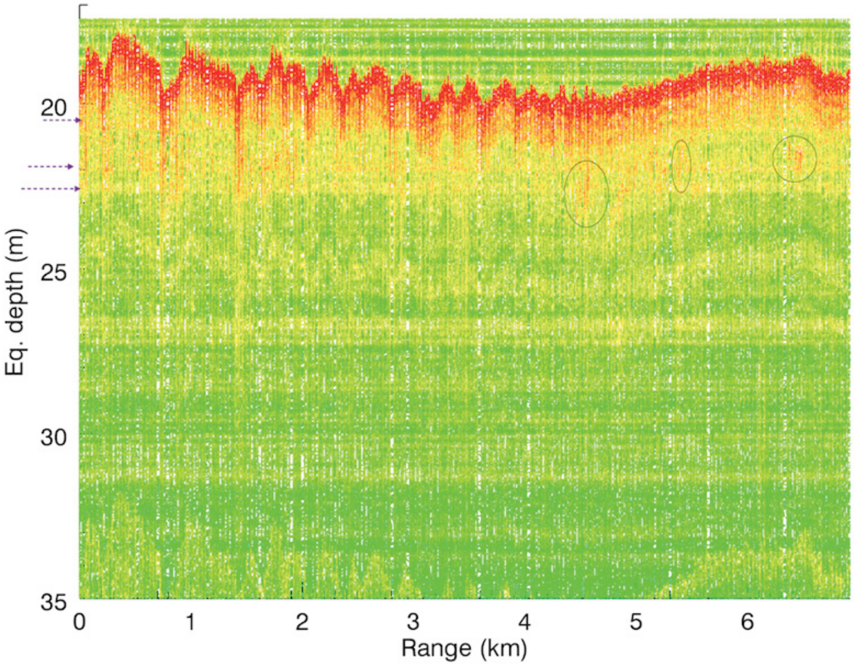

Fig. 5.1.: Image of scattering strength measured by the sub-bottom profiler along the main track in the shore parallel direction. Arrows indicate sediment layers that may cause volume scattering and the circled areas depict examples of possible discrete scatterers that may contribute to the volume scattering.

5.2 Quantitative volume scattering analysis

5.2.1 Methods

Volume scattering strength is defined as the ratio of the intensity of sound scattered by a unit area or volume to the maixmum signal intensity [3]. To calculate volume scattering from the sub-bottom profiler a method similar to that used by Leblanc [39] has been employed. In this method the volume scattering strength at a given time can be calculated using the sonar equation for incoherent scattering.

$$Sv = RL_{sv} - SL + 2TL - 10log_{10}V \tag{5.1}$$

Where Sv is the scattering strength in dB, RL_{sv} is the received scattering intensity in dB, 2TL is the the two-way transmission loss in dB, and V is the ensonified volume. Note that since the sub-bottom profiler collects reflected data the scattering received level (RL_{sv}) is calculated as SL-RL. By computing the scattering this way we are assuming that there in no refraction. It is acceptable to make such an assumption because sound speed should be increasing with depth due to compaction and therefore at a certain depth all of the refracted waves will be reflected upwards. The ensonified volume from the sub-bottom profiler is large (approximately $1000m^3$), making this assumption appropriate for this case. The two-way transmission loss was calculated using two different spreading loss laws: a spherical spreading correction and a practical spreading correction. Spherical spreading generally occurs in the water column. For two-way spreading loss it is calculated as $40 \log_{10} r$ (where r is range). However, in the sediment the two-way transmission loss is more appropriately estimated as cylindrical spreading, which is calculated as $20 \log_{10} r$. Since the sound waves are interacting with both the water column and seafloor a practical spreading loss law can be used [40]. A practical spreading loss law chooses a spreading loss constant somewhere between 40 and 20. In this report two different practical spreading loss laws were chosen. The first was a common practical spreading loss value of 30, the second value was 33.2. The second value was chosen because the ratio of distance that the wave travels through the water column to the sediment is approximately 19:10. Using this ratio a weighted average of the spreading law constant was calculated to be 33.2. An expression for absorption within the ocean was calculated using the following equation $2. * 0.002475 * r$ [3]. The ensonified volume was calculated using beam width (ψ), pulse length (τ), speed of sound in water (c), and range from the transducer (r).

$$V = \psi \frac{c\tau}{2} r^2 \tag{5.2}$$

The beam width (θ) was converted from degrees to distance (m) using the following equation.

$$\psi = 2\pi(1 - \cos\frac{\theta}{2}) \tag{5.3}$$

Since the ensonified volume is approximately 1000 m^3 the ensonified depth is approximately 10m. Therefore to calculate scattering, the reflection within a 10m depth interval of the envelope function of each trace were identified. These traces were then interpolated to a regularly spaced grid and they were then averaged over a ten meter range interval, allowing the model to compute the average scattering within an ensonified volume. The average scattering strength coefficient was calculated by averaging all of the average scattering strengths within an ensonified volume. However, the first 10 cm of the sediment was not included in the calculation because at the sediment-water interface it is roughness scattering which causes the scattering and thus these values should not be used in the calculation of volume scattering. To convert from average scattering strength to average volume scattering coefficient the following equation was used $\sigma_2 = 10^{(\frac{Sv}{10})}$. This average scattering strength coefficient was inputted into the CRA model in place of the empirically estimated volume scattering parameter. The scattering strength calculated in this section was compared to the scattering measured by a multi-beam sonar operating at 400kHz (collected and processed by Christian de Moustier). Direct location comparisons cannot be conducted because the scattering measurements were limited to just a few areas on the track and were collected nearly parallel to the direction of which the sub-bottom profiler data was collected. Despite these limitations comparing the seafloor scattering from the sub-bottom profiler to the scattering measured at high frequencies allows for a preliminary test for a frequency variation in the sediment. Since the scattering strength was measured on relatively small tracks of 200-250 m the average scattering strength calculated was plotted at 200 m intervals.

5.2.2 Results

The comparison of the calculated and measured scattering strength can be observed in Figure 5.2. It appears that the scattering calculated from the sub-bottom profiler is highly dependent on the spherical spreading correction. If the spherical spreading law of 30 is used than the scattering from the sub-bottom profiler is much lower than those measured by the multi-beam profiler. However, if the constant of 33.2 is used for the spherical spreading correction then the sub-bottom profiler has a slightly lower scattering strength than that measured by the multi-beam profiler. Volume scattering determined by the spherical spreading constant is higher than that measured by the multi-beam. The multi-beam data was processed using a spherical spreading correction, and thus, in this case, it is likely the best comparison. Note that the scattering calculated from the sub-bottom profiler has much smaller fluctuations than those measured by the multi-beam. This is likely because the sub-bottom profiler values are averages rather than directly measured. The average volume volume scattering parameter was calculated to be 0.31 using the spherical spreading calculation, 0.037 for the weighted average spherical spreading and 0.014 for the average spreading loss. Figure 5.3 shows the results from the CRA model using these calculated values (rather than empirical) of the volume scattering coefficient. As expected these models indicate that volume scattering is the dominant scattering mechanism and has a grazing angle response similar in shape to that observed in the original CRA model. The CRA plot using the volume scattering parameter 0.037 has a slightly higher scattering strength, with an intercept of -7.7 dB. The intercept increases significantly to 0.6dB when the spherical spreading correction is used. The CRA plot using the volume scattering parameter 0.014 has a lower intercept scattering strength, with an intercept of -10.7 dB.

Figure 5.4 shows the lateral spatial variation of the average scattering strength within an ensonified volume using both the spherical spreading correction (a) and the practical spreading correction of 33.2 (b). Note that since these figures have been averaged with depth and are thus two-dimensional: the depth has only been shown in order to compare the average scattering strength within an ensonified volume as a function of bathymetry. There does not seem to be any obvious relationship between high scattering values and the peaks or troughs of the bathymetry. Large average scattering values appear equally as often in both the peaks and the troughs. However, in many areas it does seem that there are scattering peaks within the transition zones between crests and troughs.

In order to get a more in depth visualization of the scattering occurring with depth the scattering strength points (before averaging) using the weighted average practical spreading law (33.2) have been plotted with the bathymetry along the main track in Figure 5.5. Although Figure 5.5 does not show any strong correlations between maximum scattering strength and the bottoms of the troughs, a pattern of peak scattering distribution does emerge. As indicated by the grey boxes it appears that there is a high concentration of discrete scatterers at approximately 4-6m below the seafloor. It is important to note that this may not be the true depth of the scatterers themselves because the peak scattering strength appears between the first and second bottom multiples. Although we do not know the exact depth of these volume scatters, we are able to determine their lateral location with reasonable certainty. These discrete scatterers appear consistently in the transition zones between the sand dune peaks and troughs. Although these discrete scatterers do not appear directly below the trough's minima they do appear within the troughs.

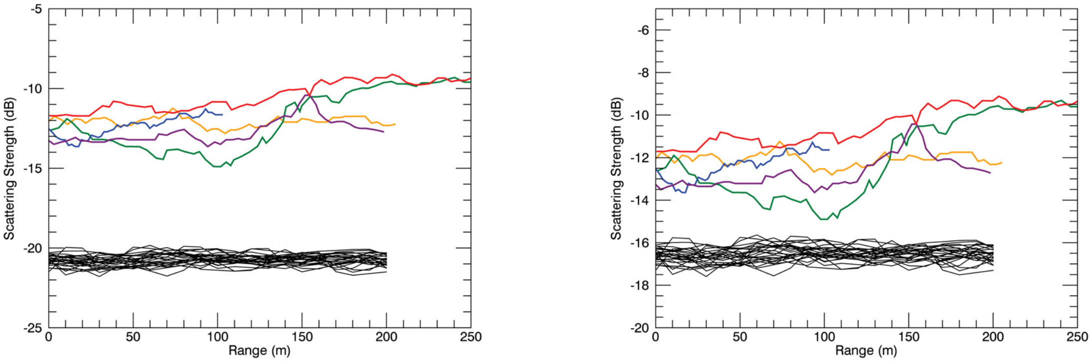

(a) Comparison of multi-beam scattering(coloured lines) and sub-bottom profiler scattering calculated with a practical spreading loss of 30

(b) Comparison of multi-beam scattering(coloured lines) and sub-bottom profiler scattering calculated with a practical spreading loss of 33.2

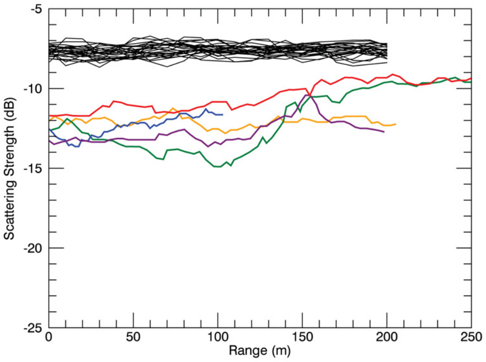

(c) Comparison of multi-beam scattering(coloured lines) and sub-bottom profiler scattering calculated with spherical spreading

Fig. 5.2.: Comparison of high-frequency scattering measurements made by a multi-beam profiler and mid-frequency scattering as calculated from the sub-bottom profile.

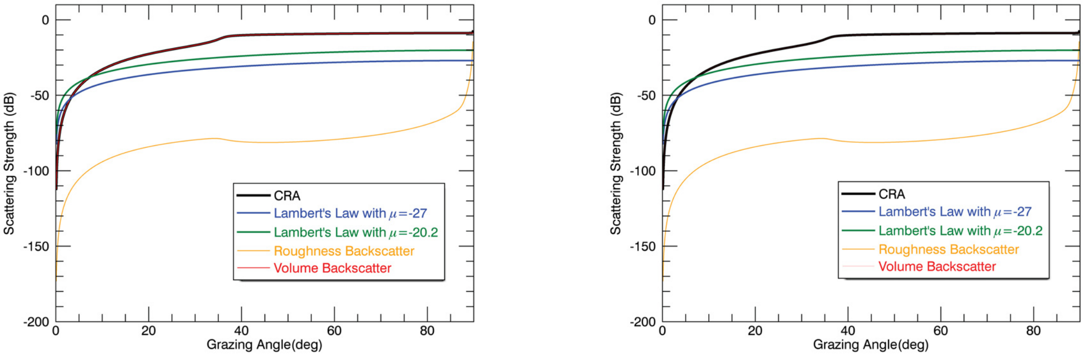

(a) CRA model computed using a volume scattering parameter of 0.31

(b) CRA model computed using a volume scattering parameter of 0.037

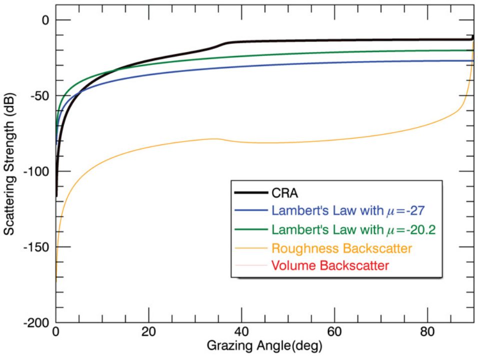

(c) CRA model computed using a volume scattering parameter of 0.037

Fig. 5.3.: Scattering strength as function of grazing angle for the CRA model computed with various different volume scattering parameters. These plots are compared to the Lambert's Law($\mu = -27$) and Lambert's Law fit for sandy sediment($\mu = -20.2$). Also shown is the roughness interface scattering strength and the volume scattering strength components computed for the CRA.

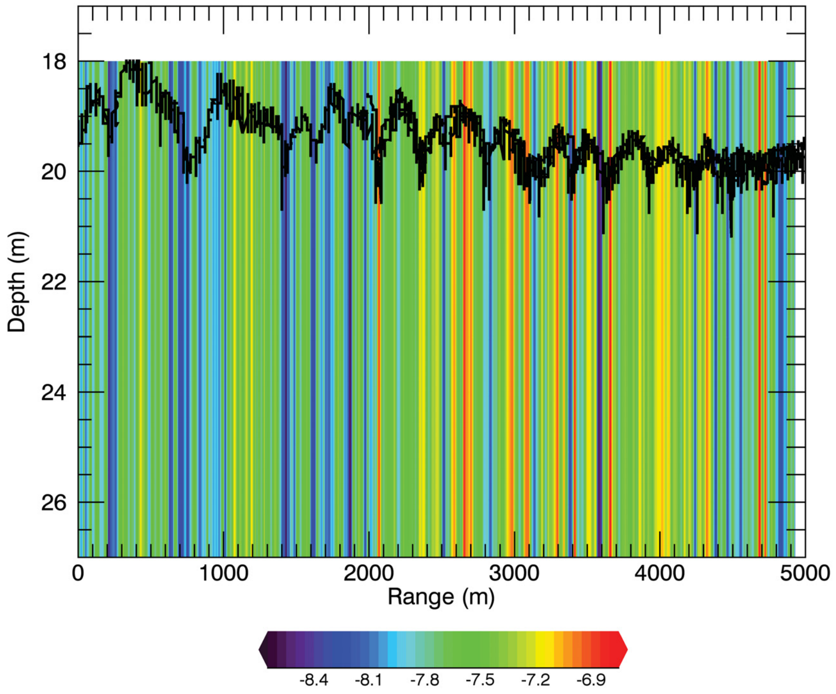

(a) Scattering within an ensonified volume using the spherical spreading law

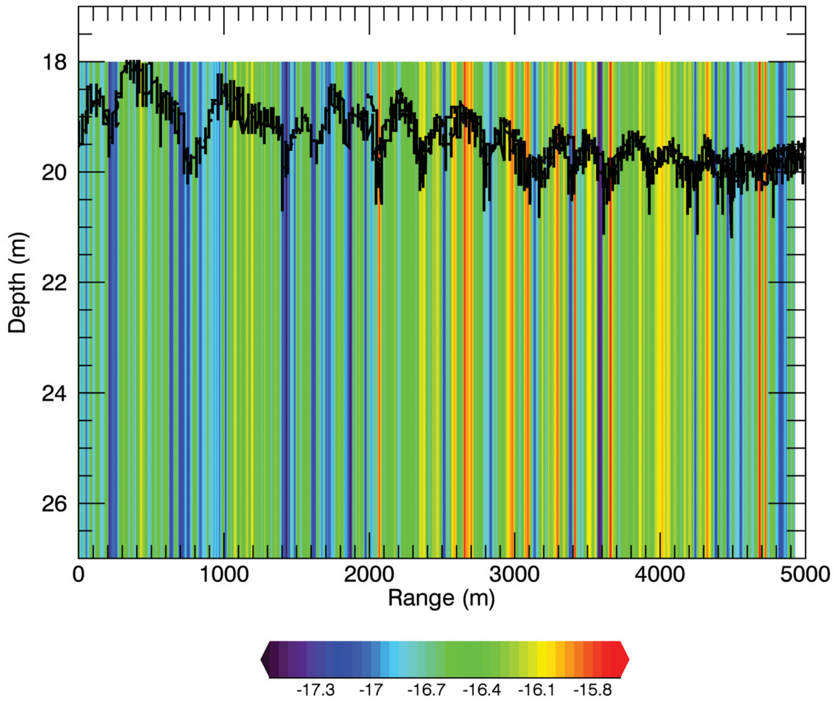

(b) Scattering within an ensonified volume using a practical spreading law of 33.2

Fig. 5.4.: Spatial variation of average scattering strength within an ensonified volume along the main track.

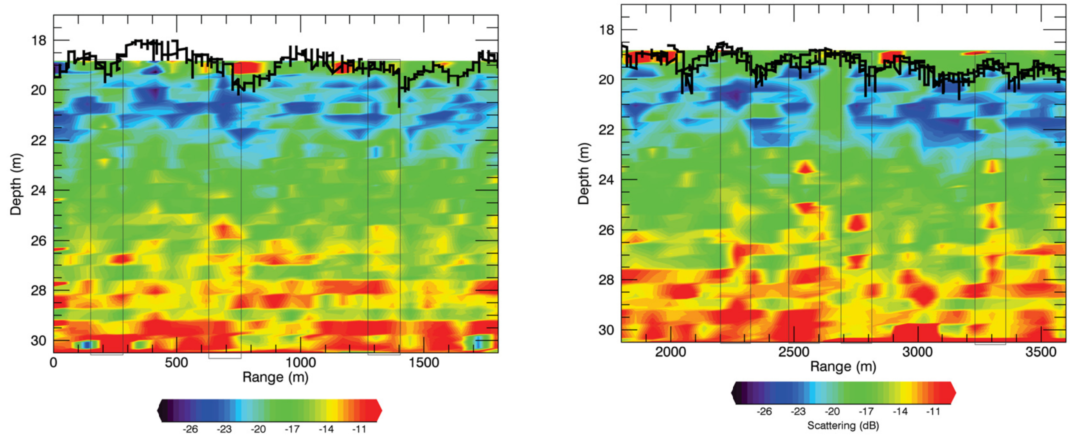

(a) Scattering strength 0-1.8km along track (b) Scattering strength 1.8-3.6km along track

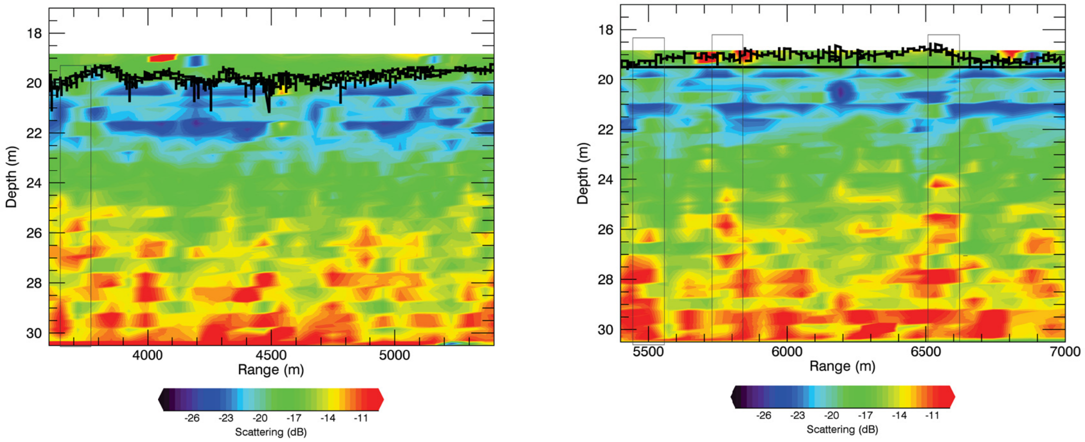

(c) Scattering strength 3.6-5.4km along track (d) Scattering strength 5.4-7km along track

Fig. 5.5.: Scattering variation of strength as a function of depth and distance along the main track. The track has been split into four sections in order to be able to see a more detailed view of potential scattering mechansims.

6. REVERBERATION MODEL

6.1 Methods

Before the total reverberation was calculated the bottom reverberation was determined for all four scattering models produced. By comparing all four bottom reverberation sub-models with measured bottom reverberation we can determine if any of the bottom reverberation models produced are sufficient enough for use in the total reverberation model. Both the bottom reverberation and the total reverberation model were computed using Espresso software. The Espresso software computed reverberation utilizing 11 sub-models. The organization of the sub-models can be observed in Figure 6.1. In addition to computing the volume reverberation, bottom reverberation, and surface reverberation the model also includes a correction for noise. The noise level is the noise received by the sonar, and it is a function of the ambient noise and platform noise. In this case the noise was calculated as the amount received relative to the amount of noise at 15 kts windspeed.

The total reverberation model of ocean volume scattering is calculated as a function of propagation loss. Propagation loss is calculated from absorption, bottom reflection, and surface reflection. It is important to note that losses due to scattering from biological life is not included in this model. The absorption was calculated using the Fisher Simmons method [41]. Bottom reflection was calculated using the APL94 guidelines [35] which uses a modified Rayleigh reflection coefficient. The Rayleigh reflection coefficient is modified by using a complex wavenumber in the sediments [41]. Surface reflection was also calculated based off of the APL94 guidelines. In APL94 a forward loss model is used to calculate surface reflection. Note that this method has been validated over the 10-100kHz range, however there have not been enough studies to validated it over the frequencies used in this study [41]. The bottom reverberation

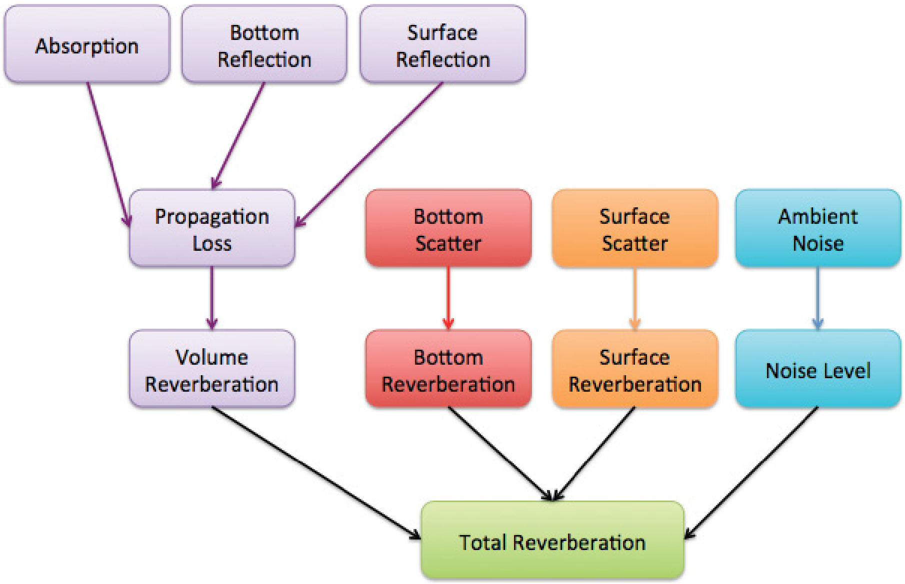

Fig. 6.1.: The organization and flow of sub models required for the reverberation model.

is calculated using the backscatter calculated in Section 4.2.1. Similar to the bottom reverberation the surface reverberation is calculated based off of the surface scatter. In this model surface scatter was calculated using the APL94 guidelines, which calculates backscatter due to near-surface bubbles. Once again this model has only been validated between 10-100 kHZ range and in the future it should be tested for its applicability to mid-frequencies. The volume, bottom, and surface reverberation were all calculated using the beam tracing method.

6.2 Results

A plot of the four models for reverberation along with 10 sets of measured reverberation have been plotted in Figure 6.2. Although the CRA model using the empirical estimate of σ_2=0.02 approximates the bottom reverberation data fairly well, the model using the weighted average practical spreading law ($\sigma_2 = 0.037$) displays a much better fit. When the $\sigma_2 = 0.037$ scattering model follows the measured data nearly perfectly, running through the centre (average) of the pings for the first four seconds. After four seconds the model drops off slightly away from the data. The models using the spherical spreading loss ($\sigma_2 = 0.31$) and the general practical spreading loss ($\sigma_2 = 0.014$) predict to high and to low values of bottom reverberation respectively.

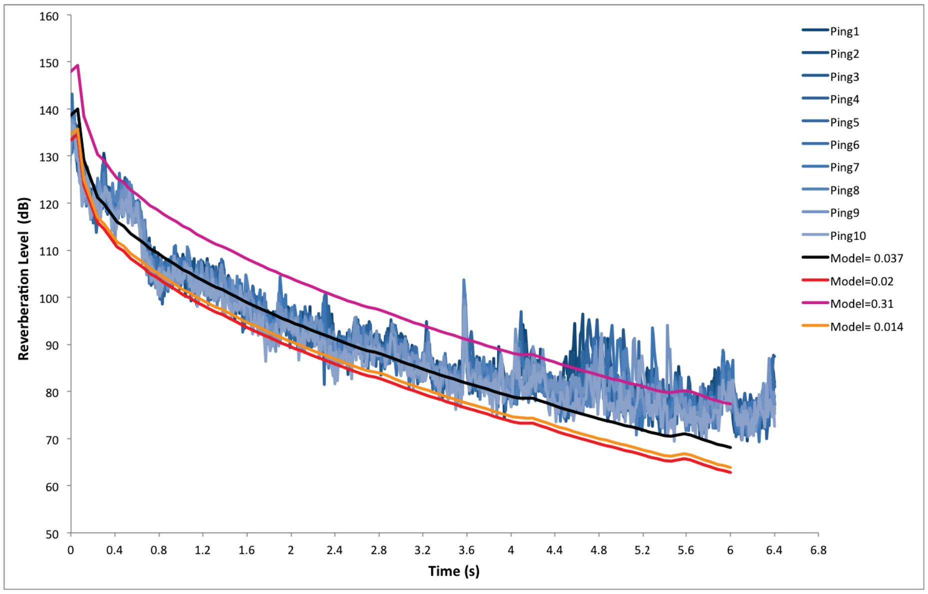

Fig. 6.2.: Comparison of measured reverberation across 10 pings and the four different models. The bottom reverberation model was calcualted using the versions of the CRA model: Red is CRA model with the empirical volume scattering parameter (0.02), orange is the CRA model with volume backscatter calculated using the spherical spreading law, pink is the CRA model with volume backscatter calculated using the practical spreading loss law, and black is the CRA model with volume backscatter calculated using the weighted average practical spreading loss law.

Since the weighted average practical spreading law model had the best fit to the bottom reverberation it was used in the calculation of the total reverberation, which can be observed in Figure 6.3. The model fits the data fairly well as an approximation, however there is many areas where the model and data diverge. The model underestimates the initial amount of reverberation by over 20 dB, but it quickly conforms to the data within 0.2 seconds. After this the data begin to diverge again, with the model decaying at a slower rate than the measured reverberation. Eventually the measured reverberation bottoms out at approximately 60 dB, however the model continues to decrease, leading to an overall difference of 10 dB by the end of the six seconds measured.

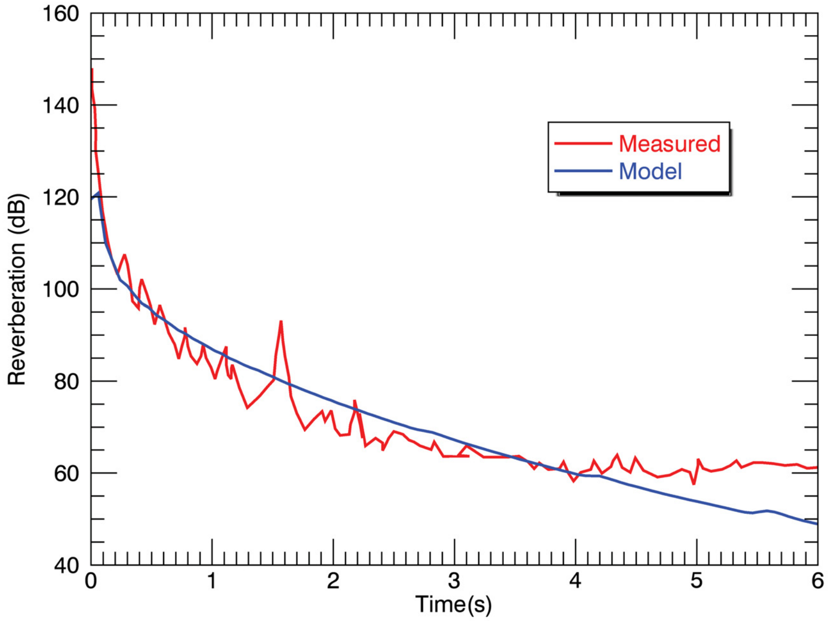

Fig. 6.3.: Reverberation level measured during TREX13 compared to reverberation model using the bottom scattering sub-model calculated with volume scattering parameter determined with the weighted spreading loss law.

7. DISCUSSION

The aim of this study was to test the applicability of current backscatter and reverberation models for mid-frequencies. The CRA model itself seems to work well as a mid-frequency backscattering model as long as the volume scattering strength is calculated rather than estimated using the empirical value. Thus the greatest constraint of the CRA model's applicability to mid-frequencies is our ability to determine volume scattering strength. The importance of the volume scattering strength is highlighted in both the CRA plot itself and in the comparison of the measurement of high-frequency scattering from the multi-beam and the mid-frequency scattering derived from the sub-bottom profiler reflection data. Each CRA scattering model produced (regardless of which volume scattering strength used) indicates that the dominant scattering mechanism is volume scattering. This can likely be attributed to the physical aspects incorporated into the model: the spectral strength and slope, calculated from the bathymetry, is used by the model to calculate the interface roughness scattering. A high spectral slope, such as that calculated for this study, indicates a smooth surface. Since the CRA model uses this value it correctly predicted the interface roughness scattering to be relatively insignificant compared to the volume scattering. A similar observation can be derived from the comparison of scattering strength determined from the multi-beam profiler and the sub-bottom profiler. The frequencies used by the multi-beam profiler are so high (300 kHz) that we can assume that it represents the roughness interface scattering and since the first 30 cm of the sub-bottom profiler data was not included in the calculation of scattering it represents the volume scattering component. When the spherical spreading correction is used for both sets of data we see that the volume scattering is significantly higher than the roughness interface scattering.

The CRA model for scattering can only produce a fair approximation of bottom reverberation. However, the bottom reverberation model produced using volume scattering that was calculated with the weighted average practical spherical spreading loss law produces a bottom reverberation model that fits the data significantly well, and doesn't start to deviate until later times. When this new bottom reverberation model is used to calculate the total reverberation the model fits well as a first approximation, however, in some areas it deviates significantly from the measured reverberation. Since the bottom reverberation model was very successful in predicting bottom reverberation we can conclude that the bottom reverberation model is contributing very little to no error in the total reverberation model. This indicates that either the environmental information provided to the model are insufficient or as discussed previously, some of the other sub-models utilized have not been validated for mid-frequencies, and thus they may not be applicable to mid-frequencies. The former is highly likely, particularly with the volume reverberation sub-model. One of the greatest contributors to ocean volume reverberation is the presence of biological life such as fish [42]. During the TREX13 sea trial a large abundance of fish were attracted to the experimental equipment which likely caused a significant amount of volume scattering. However, since the number of fish were not quantified their effect was not accounted for in the model. Thus the fish are likely the major contributor to the lack of agreement between the model and the measured data. The abundance of fish may explain why the model has such a small initial reverberation. Since the fish are in the water column they will likely scatter the sound before the seafloor, acting as an important contributor to the beginning of the reverberation curve. Note that all of the measured reverberation curves presented have curves that drop steeply in the beginning and then smoothly towards the end. According to Urick [3] this is due to the fact that in shallow water there is successive repeated bounces of sound between the seafloor and the surface that are crowded together in time, occurring shortly after the sonar emission pulse. These bounces generally quickly decay over time. The bottom reverberation model seems to mimic this behaviour well, however the total reverberation model appears to continuously drop steeply with minimal smoothing at the end. There are two possible explanations for this incorrect behaviour of the model. The first is, once again, one of the sub-models is not accurate for mid-frequencies. The sub-model that largely controls this behaviour is the spreading loss sub-model, and thus future studies should investigate this model. The second possible explanation is that the reverberation model assumes there is no multiple reverberation, however, since this experiment was conducted in shallow water it is possible that multiple reverberation is occurring, causing the measured reverberation to be much higher at the end of the reverberation time than that predicted by the sub model [3].Overall the greatest limitation on further interpretation of the reverberation modelling is the lack of validation of the sub-models and their assumptions Thus, in order to perform a complete analysis on this model, it is crucial that all the other sub-models are validated for mid-frequencies.

Since our bottom reverberation model is predicting bottom reverberation accurately we can assume that the calculated volume scattering inputs were correct and thus mapping this scattering should tell us something about the sub-bottom. The contour maps of scattering spatial variation are difficult to understand, reflecting the complications that become introduced when operating sonar at mid-frequencies. Despite this, the maps of spatial scattering do propose some possible explanations for the seemingly contradictory reverberation patterns measured during the TREX13 sea trial. The backscattering peak amplitudes were not found directly at the bottom of the troughs, however, they do often appear to be contained within the troughs, in the transition zone between the peaks and troughs of the sand dunes. Although there is also some obvious scattering from the sediment layers, these seem to be laterally homogeneous, and hence can't explain the differences between the scattering and reverberation in peaks and troughs. However, at a few meters depth there appears to be a high concentration of discrete scatterers. These scatterers are generally located below the transition zones of the sand dune waves and troughs. Thus the spatial variation in reverberation may be contributed to the presence of discrete scatters below the sediment surface. It is important to note that, due to the scattering peaks being located between the first and second water bottom multiple we cannot determine the precise depth at which these volume scatterers are located. Based off the round rather than layered nature of the discrete scatterers as well as the literature presented in Chapter 3 it is likely that the discreet scatterers are shell hash ,which cores by Goff et. al. [15] were found between 2-4 m below the sea floor.

8. CONCLUSION

The purpose of this study was to test the validity of a high-frequency backscattering and reverberation model to low frequencies using TREX13 environmental data. As expected, results from the CRA model and comparison of roughness interface scattering and calculated volume scattering indicate that volume scattering is the dominant scattering mechanism. It appears that the primary control of the spatial variation in reverberation in the northern Gulf of Mexico may be discrete scatterers within the sediment. The division of the scattering strength into its interface roughness and volume scattering components allows the CRA to be easily adjusted for mid-frequencies. However, since the CRA model determines the volume scattering empirically its use at mid-frequencies is limited to situations where the volume scattering parameter can be calculated. Since calculating the volume scattering parameter is not a very accessible option due to its high uncertainties and requirements of sub-bottom profiler data, I suggest that future studies focus on adapting the CRA model so that it calculates the volume scattering parameter using physical approximations. Since it is likely that the presence of discrete scatterers are important contributor to scattering at mid-frequencies it is important that future work focuses on discrete scattering modelling.

Multiple different modified CRA models were produced from calculating the volume scattering using several different spreading loss laws. The weighed average spherical spreading loss law producing the best fit to the measured bottom reverberation data. Despite this adjustment to the bottom reverberation model, there are still significant differences between the modelled and measured total reverberation. This lack of agreement indicates there are a number of pertinent adjustments required to adapt the total reverberation model for mid frequencies. The future work involved with this would likely include adding opportunities to quantify scattering mechanisms not included in the current model such as the presence of biological life. There is also a great deal of future work needed to verify that all the sub-models and assumptions used in the total reverberation model are applicable to mid-frequencies.

LIST OF REFERENCES

LIST OF REFERENCES

[1] D. Jackson and M. Richardson, *High-Frequency Seafloor Acoustics*. The Underwater Acoustics Series, Springer New York, 2007.

[2] H. Medwin and C. S. Clay, *Fundamentals of acoustical oceanography*. Academic Press, 1998.

[3] R. J. Urick, *Principles of underwater sound*. McGraw-Hill, 1983.

[4] K. S. Davis, N. C. Slowey, I. H. Stender, H. Fiedler, W. R. Bryant, and G. Fechner, "Acoustic backscatter and sediment textural properties of inner shelf sands, northeastern gulf of mexico," *Geo-Marine Letters*, vol. 16, pp. 273–278, sep 1996.

[5] D. Tang, K. Briggs, K. Williams, D. Jackson, E. Thorsos, and D. Percival, "Fine-scale volume heterogeneity measurements in sand," *IEEE Journal of Oceanic Engineering*, vol. 27, pp. 546–560, jul 2002.

[6] A. I. Konyukhov, "Geological structure, evolution stages, and petroliferous complexes of the gulf of mexico basin," *Lithol Miner Resour*, vol. 43, pp. 380–393, jul 2008.

[7] A. Hine, S. Dunn, and S. Locker, "Geologic beginnings of the gulf of mexico with emphasis on the formation of the de soto canyon, deep-c consortium," 2013.

[8] O. Wilhelm and M. Ewing, "Geology and history of the gulf of mexico," *Geol Soc America Bull*, vol. 83, no. 3, p. 575, 1972.

[9] S. J. Williams, J. Flocks, C. Jenkins, S. Khalil, and J. Moya, "Offshore sediment character and sand resource assessment of the northern gulf of mexico, florida to texas," *Journal of Coastal Research*, vol. 60, pp. 30–44, may 2012.

[10] W. W. Sager, I. R. MacDonald, and R. Hou, "Geophysical signatures of mud mounds at hydrocarbon seeps on the louisiana continental slope, northern gulf of mexico," *Marine Geology*, vol. 198, pp. 97–132, jun 2003.

[11] D. McGookey, "Gulf coast cenozoic sediments and structure: An excellent example of extra-continental sedimentation," *Gulf Coast Association of Geological Societies Transactions*, vol. 25, pp. 104–120, 1975.

[12] H. R. Gould and R. H. Stewart, "Continental terrace sediments in the northeastern gulf of mexico," pp. 2–20, 1955.

[13] W. L. Balsam and J. P. Beeson, "Sea-floor sediment distribution in the gulf of mexico," *Deep Sea Research Part I: Oceanographic Research Papers*, vol. 50, pp. 1421–1444, dec 2003.

[14] L. Doyle and P. Feldhausen, "Bottom sediments of the eastern gulf of mexico examined with traditional and multivariate statistical methods," *Journal of the International Association for Mathematical Geology*, vol. 13, no. 2, pp. 93–117, 1981.

[15] J. A. Goff, "Reconnaissance marine geophysical survey for the shallow water acoustics program," 2013.

[16] A. H. Bouma, H. H. Roberts, and J. M. Coleman, "Acoustical and geological characteristics of near-surface sediments, upper continental slope of northern gulf of mexico," *Geo-Marine Letters*, vol. 10, pp. 200–208, dec 1990.

[17] A. Goldstien, "Sedimentary petrologic provinces of the northern gulf of mexico," *Sed. Petrol*, vol. 12, no. 2, pp. 77–84, 1942.

[18] G. M. Griffin, "Regional clay-mineral facies—products of weathering intensity and current distribution in the northeastern gulf of mexico," *Geol Soc America Bull*, vol. 73, no. 6, p. 737, 1962.

[19] P. Fleischer, W. B. Sawyer, H. Fiedler, and I. H. Stender, "Spatial and temporal variability of a coarse-sand anomaly on a sandy inner shelf, northeastern gulf of mexico," *Geo-Marine Letters*, vol. 16, no. 3, pp. 266–272, 1996.

[20] L. J. Doyle and T. N. Sparks, "Sediments of the mississippi, alabama, and florida (mafla)continental shelf," *Journal of Sedimentary Petrology*, vol. 50, no. 3, pp. 905–915, 1980.

[21] J. Ludwick, "Sediments in northeastern gulf of mexico," *Studies in Marine Geology with Implications in Earth History*, pp. 204–238, 1964.

[22] S. J. PARKER, A. W. SHULTZ, and W. W. SCHROEDER, "Sediment Characteristics and Seafloor Topography of a Palimpest Shelf, Mississippi-Alabama Continental Shelf," in *Quaternary Coasts of the United States*, pp. 243–251, Society for Sedimentary Geology, 1992.

[23] B. Kraft, C. de Moustier, B. Calder, and L. Mayer, "High-resolution mapping and backscatter studies in support of the ripples program," *The Journal of the Acoustical Society of America*, vol. 120, no. 5, p. 3180, 2006.

[24] B. J. Kraft and C. de Moustier, "Detailed bathymetric surveys offshore santa rosa island, FL: Before and after hurricane ivan (september 16, 2004)," *IEEE Journal of Oceanic Engineering*, vol. 35, pp. 453–470, jul 2010.

[25] A. H. Reed, K. E. Thompson, K. B. Briggs, and C. S. Willson, "Physical pore properties and grain interactions of SAX04 sands," *IEEE Journal of Oceanic Engineering*, vol. 35, pp. 488–501, jul 2010.

[26] R. Mickey, K. Xu, S. Libes, and J. Hill, "Sediment texture, erodibility, and composition in the northern gulf of mexico and their potential impacts on hypoxia formation," *Ocean Dynamics*, vol. 65, pp. 269–285, dec 2014.

[27] M. Buckingham and M. Richardson, "On tone-burst measurements of sound speed and attenuation in sandy marine sediments," *IEEE Journal of Oceanic Engineering*, vol. 27, pp. 429–453, jul 2002.

[28] M. Richardson, K. Briggs, L. Bibee, P. Jumars, W. Sawyer, D. Albert, R. Bennett, T. Berger, M. Buckingham, N. Chotiros, P. Dahl, N. Dewitt, P. Fleischer, R. Flood, C. Greenlaw, D. Holliday, M. Hulbert, M. Hutnak, P. Jackson, J. Jaffe, H. Johnson, D. Lavoie, A. Lyons, C. Martens, D. McGehee, K. Moore, T. Orsi, J. Piper, R. Ray, A. Reed, R. Self, J. Schmidt, S. Schock, F. Simonet, R. Stoll, D. Tang, D. Thistle, E. Thorsos, D. Walter, and R. Wheatcroft, "Overview of SAX99: environmental considerations," *IEEE Journal of Oceanic Engineering*, vol. 26, no. 1, pp. 26–53, 2001.

[29] K. Briggs, A. Reed, D. Jackson, and D. Tang, "Fine-scale volume heterogeneity in a mixed sand/mud sediment off fort walton beach, fl," *IEEE Journal of Oceanic Engineering*, vol. 35, no. 3, pp. 77–84, 2010.

[30] T. Pyle, V. McCarthy, R. Gile, and T. Neubauter, "Baseline monitoring studies, mississippi, alabama, florida, outer continental shelf, 1975-1976,v.v. geophysical investigations for biolithologic mapping of the mafla-ocs lease area," pp. 30–44, 1976.

[31] S. S, K. Briggs, P. Fliesher, R. Ray, and W. Sawyer, "Shallow-water high-frequency bottom scattering off panama city, florida," *J. Acoust. Soc. Am.*, vol. 85, pp. 2134–2144, 1988.

[32] P. Fleischer, W. B. Sawyer, H. Fiedler, and I. H. Stender, "Spatial and temporal variability of a coarse-sand anomaly on a sandy inner shelf, northeastern gulf of mexico," *Geo-Marine Letters*, vol. 16, pp. 266–272, sep 1996.

[33] M. D. Richardson and K. B. Briggs, "In situ and laboratory geoacoustic measurements in soft mud and hard-packed sand sediments: Implications for high-frequency acoustic propagation and scattering," *Geo-Marine Letters*, vol. 16, pp. 196–203, sep 1996.

[34] F. Francisca, T.-S. Yun, C. Ruppel, and J. Santamarina, "Geophysical and geotechnical properties of near-seafloor sediments in the northern gulf of mexico gas hydrate province," *Earth and Planetary Science Letters*, vol. 237, pp. 924–939, sep 2005.

[35] "Apl-uw high-frequency ocean environmental acoustic models handbook," tech. rep., Dod, Defense Technical Information Center, 1995.

[36] S. Stoll, Y. Sun, and I. Bitte, "Seafloor properties from penetrometer tests," *IEEE Journal of Oceanic Engineering*, vol. 32, no. 1, pp. 57–63, 2007.

[37] K. Kim, M. Prezzi, and R. Salgado, "Interpretation of cone penetration tests in cohesive soils," 2006.

[38] D. Mosher, H. Christian, D. Cunningham, K. MacKillop, A. Furlong, and K. Jarrett, "The harpoon free fall cone penetrometer for rapid offshore geotechnical assesment," *International Conference on Offshore Site Investigation and Geotechnic*, 2007.

[39] L. R. Leblanc, "Erratum: High-resolution sonar volume scattering measurements in marine sediments," *The Journal of the Acoustical Society of America J. Acoust. Soc. Am.*, vol. 99, p. 1259, May 1995.

[40] A. D. Jones, A. J. Duncan, D. W. Bartel, A. Zinoviev, and A. Maggi, "Practical spreading laws: The snakes and ladders of shallow water acoustics," *UAM Proceedings*, 2011.

[41] N. U. R. Center, "Espresso software manual," 2008.

[42] P. C. Etter, *Underwater acoustic modeling: principles, techniques, and applications.* Elsevier Applied Science, 1991.